Homeostatic maintenance and age-related functional decline in the Drosophila ear

Homeostatic maintenance and age-related functional decline in the *Drosophila* ear

Alyona Keder[1], Camille Tardieu[1], Liza Malong[1], Anastasia Filia[2], Assel Kashkenbayeva[1], Fay Newton[3], Marcos Georgiades[1], Jonathan E. Gale[1], Michael Lovett[2], Andrew P. Jarman[3] & Joerg T. Albert[1,4,5,6,7]*

Affiliations:

[1]Ear Institute, University College London, 332 Gray's Inn Road, London WC1X 8EE, UK

[2]National Heart and Lung Institute, Imperial College London, Guy Scadding Building, Dovehouse 9 Street, London, SW3 6LY, UK

[3]Centre for Discovery Brain Sciences, Edinburgh Medical School, University of Edinburgh, Edinburgh EH8 9XD, Scotland, UK

[4]Centre for Mathematics and Physics in the Life Sciences and Experimental Biology (CoMPLEX), University College London, Gower Street, London WC1E 6BT, UK

[5]The Francis Crick Institute, 1 Midland Road, London NW1 1AT, UK

[6]Department of Cell and Developmental Biology, University College London, Gower Street, London WC1E 6DE, UK

[7]Lead Contact

*Correspondence to: joerg.albert@ucl.ac.uk

Abstract (150 words):

Age-related hearing loss (ARHL) is a threat to future human wellbeing. Multiple factors contributing to the terminal auditory decline have been identified; but a unified understanding of ARHL - or the homeostatic maintenance of hearing before its breakdown - is missing. We here present an in-depth analysis of homeostasis and ageing in the antennal ears of the fruit fly *Drosophila melanogaster*. We show that *Drosophila*, just like humans, display ARHL. By focusing on the phase of dynamic stability prior to the eventual hearing loss we discovered a set of evolutionarily conserved homeostasis genes. The transcription factors Onecut (closest human orthologues: ONECUT2, ONECUT3), Optix (SIX3, SIX6), Worniu (SNAI2) and Amos (ATOH1, ATOH7, ATOH8, NEUROD1) emerged as key regulators, acting upstream of core components of the fly's molecular machinery for auditory transduction and amplification. Adult-specific manipulation of homeostatic regulators in the fly's auditory neurons accelerated - or protected against - ARHL.

Introduction

A surface calm can be misleading. All living things, from unicellular amoeba to neurons in the human brain, require continual maintenance and the constant flow of their seemingly equable physiological operations is in fact the product of complex homeostatic networks. All life, it has been said, needs to run to stand still. As with many things, the underlying machinery remains largely unrecognized until it breaks down. A most pertinent example of such a breakdown are the hearing impairments that affect about 1.23 billion people worldwide, corresponding to one sixth of the world's total population [1]. The aetiology of hearing loss is diverse but the arguably single most important factor is age. Age-related hearing loss (ARHL) carries the vast bulk of the global disease burden, but no treatments, neither preventive nor curative, are currently in sight. Multiple factors have been linked to ARHL, including extrinsic (e.g. noise exposure, ototoxic drugs or smoking) as well as intrinsic (molecular, physiological) ones [2-4]. Over the past few decades, gene discovery studies using mouse models have also identified numerous candidate genes for human deafness [5-11]. Three recent larger scale screens in mice and one recent genome-wide association screen (GWAS) in humans have brought the total number of candidate hearing loss genes to 154 [12-15]. Yet, a unified view on the underlying mechanisms of ARHL, and particularly the gene-regulatory networks that mediate the maintenance of sensitive hearing throughout the lifespan, is still lacking. We here use the auditory system of the fruit fly in an attempt to shed some light on these issues.

Despite the stark anatomical differences, the ears of vertebrates and *Drosophila* also share marked similarities; these include (i) some fundamental biophysical mechanisms of auditory transduction [16] and amplification [17,18], (ii) the fact that the inner ears of flies and vertebrates host the sensors for both sound and gravity and that these also display a broadly similar architecture of neuronal pathways from the ear to higher-order centres in the brain [19] and, finally, (iii) molecularly conserved families of proneural genes that control hearing organ development, such as e.g. *ato* [20] in flies and Math1/Atoh1 in mice (or ATOH1 in humans) [21]. The various similarities and – molecularly - near identities [22,23], between the ears of *Drosophila* and vertebrates (including mammals) have recommended the fly as a powerful model to study more fundamental aspects of hearing and deafness [24], especially those around transducer-based amplification, which are facilitated in *Drosophila* due to their lack of both Prestin-mediated electromotility [25] and efferent innervation [26].

Many *Drosophila* hearing genes have been identified [24,27,28], but so far no study has explored the flies' hearing across their life course. We found that the ears of fruit flies also display ARHL; virtually all parameters of sensitive hearing start declining after 50 days of age (at 25 °C).

Taking one step back, however, we set out to identify those homeostatic regulators that maintain the fly's sensitive hearing before the onset of ARHL. We combined RNA-Seq-based transcriptomics with bioinformatical, biophysical and behavioural tools to explore the landscape of age-variable genes of the Johnston's Organ (JO) - the flies' inner ear'. Our data suggests that the thereby identified transcriptional regulators are not restricted to *Drosophila* - or the sense of hearing - but represent key players of homeostasis across taxa and possibly across sensory modalities.

Results

Drosophila is prone to age-related hearing loss (ARHL)

Functionally, the *Drosophila* antennal ear (Fig. 1a) comprises of two components: (i) the external *sound receiver* (jointly formed by the third antennal segment, A3, and its lateral appendage, the arista) and (ii) the actual *'inner ear'*, which is formed by Johnston's Organ (JO), a chordotonal organ [29] located in the second antennal segment, A2. JO harbours ~500 mechanosensory neurons [30].

To assess hearing across the *Drosophila* life course we first measured the locomotor activities of flies in response to a playback of courtship song components at different ages. *Drosophila melanogaster* males increase locomotor activity in response to courtship song [31]. While 10- and 50-day-old flies increased their locomotor activity in response to a 15 min long train of courtship song pulses (inter-pulse-interval, IPI: 40ms), sound-induced responses were absent in 60-day-old flies (Fig. 1b, left). We did, however, observe courtship behaviour (wing extension) in 60-day old males when paired with younger virgin females (data not quantified); consistent with this, so far no study has reported a cut-off age for male mating drive in Drosophilid flies. While individual parameters of male mating performance decline with age [32]; other parameters appear to increase [33], suggesting that the observed loss of response is not a loss of mating interest *per se*. Moreover, baseline locomotor activities of 60-day-old flies were the same as in 10-day-old flies (Fig. 1b, right), pointing towards an auditory - rather than a more generalised neurological - deficit as the underlying cause for the non-responsiveness to sound.

A simple, but quantitatively powerful, test of auditory performance was then conducted by recording the vibrations of unstimulated sound receivers (*free fluctuations*) [18]. A receiver's free fluctuations reveal three principal parameters of auditory function: (1) the ear's best frequency, f_0 (measured in Hz), (2) its frequency selectivity or quality factor, Q (dimensionless), and (iii) its energy - or power - gain (measured in K_BT). Much like hair cells in the vertebrate inner ear,

the antennal ears of *Drosophila* are active sensors, which inject energy into sound-induced receiver motion [34].

Our data show that the ears of flies, much like those of humans, show age-related hearing loss (ARHL) (Fig. 1c). At 25 °C, the antennal receivers of 70-day-old flies show (i) best frequency shifts towards the passive system, where no energy injection is observed, (ii) a greatly reduced tuning sharpness and (iii) a ~90% loss of their energy gains (Fig. 1c and Supplementary Table 1), indicating a near-complete breakdown of the active process - which supports hearing - at day 70. The time course of this auditory decline was broadly similar between males and females (Supplementary Table 1).

To probe auditory function in more detail, we also quantified the mechanical and electrophysiological signatures of auditory mechanotransduction in response to force-step actuation of the fly's antennal ear at different ages (Fig. 1d). Direct mechanotransducer gating introduces characteristic nonlinearities - namely drops in stiffness - into the mechanics of the sound receiver. These so-called 'gating compliances' can be modelled with a simple gating spring model [16,35] thereby allowing for calculating the number - and molecular properties - of different populations of mechanosensory ion channels present in the fly's JO [36]. Two distinct mechanotransducer populations have previously been described: a *sensitive* population, linked to hearing, and an *insensitive* population, linked to the sensation of wind and gravity [19]. At day 70, the numbers of predicted sensitive (N_s) and insensitive (N_i) channels have decreased by ~50% as compared to their values at day 1; the single channel gating forces of the sensitive (z_s) and insensitive channels (z_i), in turn, have increased (Fig. 1d). The receiver's steady-state stiffness (K_{steady}), however, which is an indicator of the integrity of the antennal joint, is not significantly different between 1- and 70-day-old flies, suggesting that the changes in auditory mechanics reflect an ageing of the mechanotransducer machinery rather than structural changes of the organ itself. Compound action potential (CAP) responses to force step actuation - recorded from the antennal nerve - showed that nerve response magnitudes initially increased from day 1 to day 25 and then decreased steadily, with response curves of 70-day-old flies falling below those of 1-day-old flies, both in response magnitude and displacement sensitivity (Fig. 1d). The above-described pattern of transducer ageing was seen in both males and females. Some subtle differences, however, could be observed between the sexes. While females displayed a ~stable baseline of most transduction parameters up to day 50, males showed signs of a steadier decline from day 1 on. Also, gating spring stiffnesses (K_{GS}) decreased in 70-day-old males but increased in 70-day-old females (Fig. 1d).

Summing up the behavioural, mechanical and electrophysiological evidence, the auditory life course of *Drosophila melanogaster* can roughly be broken down into two phases: (i) a dynamic

phase of *homeostatic metastability*, which is characterised by fluctuations of key parameters of hearing around a ~stable baseline, which last from day 1 to ~day 50 (also including possible signs of initial functional maturation) and (ii) a phase of *terminal decline*, which starts at ~day 50 and leads to a near complete loss of auditory function at ~day 70.

We hypothesized that a breakdown of the homeostatic machinery, which shapes auditory performance during the life course and maintains healthy hearing up until day 50, might be the ultimate reason for the observed terminal decline. In order to identify the molecular networks involved, we therefore profiled the auditory transcriptome at days 1, 5, 10, 25 and 50 through RNA sequencing (RNA-Seq) of the 2nd antennal segment (Supplementary Table 2).

The age-variable auditory transcriptome in *Drosophila*

16,243 genes are expressed in the 2nd antennal segment in both males and females (Supplementary Table 2); 13,324 of those are protein-coding. We compared the expression levels of all genes in a pair-wise manner, between (i) day 1 and 5, (ii) day 5 and 25 and (iii) day 25 to 50. In total, 5,855 (4,936 protein-coding) genes were changing their expression significantly in at least in one of the three pair-wise comparisons (criteria: >1.5-fold change; <10% False Discovery Rate (FDR); $p<0.05$; Supplementary Table 3 and Supplemental Methods). This first step of the analysis identified those genes that showed a significant change of expression level at any stage of the life course, irrespective of the corresponding sign of this change (up- or downregulation). 64% of all genes (10,388 of 16,243) showed constant expression levels and were ruled out at this stage.

The gene-ontological nature of age-variable genes in A2 was probed with the **G**ene **O**ntology en**RI**chment ana**L**ysis and visualization (GOrilla) tool [37,38]. The age-variable transcriptome revealed both down- and upregulation of genes. Genes involved in ATP metabolism, protein processing and structural molecules were found to be downregulated, whereas immune response genes, photo transduction genes and translation machinery genes were upregulated (Fig. 2a and Supplementary Table 4). Next to many novel JO genes, about one third (109) of all previously reported JO genes (314) [24,28] changed their expression in our dataset (Table 1); this included rhodopsins, the TRPV channel gene *nan*, innexins, as well as ATPase β subunits (nervanas) previously linked to JO function [39,40].

We also found that 67% (74 out of 111) of hearing loss genes recently identified in mice [12-14] are conserved in flies - and expressed in A2 – with 32% of them also showing age-variable expression in JO. In addition, a recent genome-wide association screen (GWAS) identified 44

new genes associated with ARHL in humans; 80% of those are conserved in flies - and expressed in A2 – with 27% being age-variable [15] (Table 2).

Number of JO neurons remains constant up until the age of 50 days

To test whether the age-variable transcriptome between day 1 and day 50 reflected changes on the cellular level we counted the number of neurons in the second antennal segment at different ages (Supplementary Fig. 1). From day 1 to day 50 no difference in neuronal numbers was seen, suggesting that the observed transcriptomic changes betray an age-variable transcriptional - i.e. gene-regulatory - activity.

Predicting the gene-regulatory landscape of auditory homeostasis in *Drosophila*

In order to shed light on the gene-regulatory networks of auditory homeostasis and identify key transcription factors (TFs) acting upstream of the age-variable genes, we applied the bioinformatics software package iRegulon, which predicts TFs based on motif binding probabilities [41].

Our heuristic rationale was based on three assumptions: (i) auditory homeostasis involves, at least in parts, specific TFs; (ii) TFs can be low abundance genes, their action can be mediated through small changes in expression levels; (iii) every TF has, on average, more than one target and those targets might be functionally, or gene-ontologically, linked.

We drew three consequences from the above premises: First, we concentrated our study on TFs. Second, we used the entire age-variable auditory regulon to *predict* upstream TFs, thereby increasing the overall sensitivity of our analysis. Even TFs, which might have escaped our attention from the RNA-Seq data itself could thus be recovered in subsequent bioinformatical analyses. Third, we grouped putative regulons (i.e. subsets of expressed genes) not only by their variability with age but also by their gene-ontological classification.

37 TFs were predicted from different rounds of gene submission (Supplementary Table 5), based on varying gene ontological categories, such as (i) transporters and receptors, (ii) trafficking genes, (ii) structural genes, (iv) most abundantly expressed genes or (v) genes most variable between ages (Fig. 2b). *Onecut*, *Optix*, *atonal* (*ato*), *Drop* (*Dr*), *cubitus interruptus* (*ci*), *Sox100B* and *PvuII-PstI homology 13* (*Pph13*) were predicted to regulate the transcription of receptors and transporters, including the key auditory ion channels NompC and Nanchung (Nan). *Absent MD neurons and olfactory sensilla* (*amos*) and *Optix* were predicted to regulate the transcription of structural genes, such as actins and tubulins (the most severely

downregulated genes (Fig. 2a). *Worniu* (wor) was predicted to be upstream of trafficking machinery, while *amos and wor* were both upstream of dynein motor protein family, that are indispensable for ion channel transport and homeostasis (Supplementary Fig. 2).

Testing predicted homeostatic regulators of *Drosophila* hearing

To test the validity, and functional relevance, of the bioinformatical analyses, we used RNAi-mediated, adult-specific knockdowns (KDs) of 19 (out of 37) predicted transcription factors: *Adult enhancer factor 1* (*Aef1*), *absent MD neurons and olfactory sensilla* (*amos*), *anterior open* (*aop*), *araucan (ara)*, *atonal* (*ato*), cut (*ct*), *glass* (*gl*), *longitudinals lacking* (*lola*), *onecut, Optix, pannier* (*pnr*), *PvuII-PstI homology 13* (*Pph13*), *regulatory factor X (Rfx)*, *runt (run), Sox box protein 14* (*sox14*), *serpent* (*srp*), *Signal-transducer and activator of transcription protein at 92E* (*Stat92E*), *TATA-binding protein* (*Tbp*) and *worniu (wor)* (Supplementary Table 6). The adult-specific knockdown was achieved by using a neuron-specific Gal4 driver line in combination with a temperature-sensitive transcriptional inhibitor of Gal4 ($Gal80^{ts}$) and the respective UAS-RNAi constructs. Transcription of RNAi constructs was initiated by transferring flies to a 30°C environment post eclosion. RNAi efficacy was validated by means of RT-qPCR and showed at least 60% reduction of gene expression (Supplementary Fig. 3). Analysing the free fluctuations of the antennal sound receiver, we found 5 cases (*onecut*, *amos*, *gl*, *lola* and *Sox14*), where the knockdown accelerated the ARHL phenotype; 4 other cases (*wor*, Optix, *Pph13* and *ara*), however, showed protective phenotypes for various principal parameters of auditory function (Supplementary Table 6). Adult-specific knockdowns of the crucial developmental genes *ato* [20], *Rfx* [42] and *ct* [43] did not show any significant phenotypic changes (Supplementary Table 6), suggesting that they are not involved in homeostatic maintenance of hearing in adults.

To get a better understanding of the specific TF-mediated homeostatic programme that maintains hearing, we concentrated on the top four regulators, which occurred consistently throughout various rounds of bioinformatical analyses. These were *onecut*, *Optix*, *wor* and *amos*, all of which showed clear expression in the neurons of JO (Fig. 3). These four TFs also showed the strongest KD phenotypes in the free fluctuation experiments (Fig. 4a, b and Supplementary Table 6), with each TF affecting distinct aspects of auditory function. Analysing the mechanical and electrophysiological signatures of mechanotransducer gating across the four KDs (Fig. 4c, d) identified *onecut* as a crucial homeostatic regulator of auditory transducer function. The number of predicted sensitive (auditory) transducer channels (N_s) is greatly reduced in *onecut* KD flies, while their single channel gating forces (z_s) are increased. The numbers of predicted insensitive (non-auditory) channels (N_i) are slightly increased and their

single channel gating forces (z_i) decreased in *onecut* KDs. The observed inverse relationship between ion channel numbers and gating forces might represent an intrinsic homeostatic link between the two parameters (see also discussion and Supplementary Fig. 3). CAP responses to force-step actuation, finally, are dramatically reduced in the KD condition. The overall effect of the adult-specific KD of *onecut* is a near-complete abolition of the mechanical and electrical signatures of sensitive auditory transducer gating. Consistent with these results, *onecut* KD flies specifically lose their responsiveness to sound, while their baseline locomotor activities remain unchanged (Fig. 4e). KDs of *Optix*, *amos* and *wor* showed less pronounced effects on electrophysiological or mechanical signatures of transducer gating, but at least one transducer parameter was affected in each genotype (Fig. 4d). Similarly to onecut KD, amos KD flies lose their responsiveness to sound, whereas KD of wor and Optix increases the sensitivity to sound, which manifests in an acoustic startle, i.e. a reduction of activity in response to sound (Fig. 4e). For three of the four master regulators (Optix, wor, amos), overexpression constructs were available, we thus also explored whether overexpression could invert the knockdown phenotypes seen in the free fluctuation analyses (compare to Fig. 4a); this was indeed the case for *Optix* and *amos*; wor overexpression was indistinguishable from controls (Supplementary Fig. 5, Supplementary Table 6). Canton-S flies show accelerated age-related hearing loss (aARHL) at 30 °C, their hearing loss after 25 days is equivalent to that of 60-day-old flies raised at 25 °C. Over-expression of *amos* or downregulation of *wor* (both 30 days at 30 °C) - led to a partial prevention of the age-related auditory decay (Fig. 5c).

qPCR validation reveals key auditory targets of master regulators

Knockdown and overexpression of identified homeostatic TFs altered important parameters of the fly's ear, such as its frequency tuning, mechanotransduction, amplification and nerve responses (Fig. 4a-d). All of these system properties are thought to arise from an interaction of three key transient receptor potential (TRP) channels, namely Nanchung (Nan) [44], Inactive (Iav) [45] and NompC [46] with motor proteins from the dynein family [27]. One such dynein was also identified within our age-variable gene set, this is the Dynein heavy chain at 98D (Dhc98D). The three TRP channels from above, as well as the auditory dyneins were predicted downstream of the four master regulators (Fig. 2b, Supplementary Fig. 2). Using real-time quantitative polymerase chain reactions (qPCRs) we therefore tested if *nan*, *iav*, *nompC* and *Dhc98D* levels were under the control of the identified homeostatic TFs (Fig. 5a). RNAi-mediated adult-specific knockdown of *onecut* resulted in a dramatic downregulation of both *nan* and *iav*, knockdown of *Optix* lead to an upregulation of *nompC* levels, whereas knockdown of *amos* and *wor* showed downregulation of *Dhc98D*.

Adult-specific knockdown of *Dhc98D* caused a strong hearing loss phenotype similar to the one seen after *amos* KD (Figs. 4a and 5b).

Discussion

We show that flies, just like humans, are prone to age-related hearing loss (ARHL). ARHL manifests in various aspects of *Drosophila* hearing function. As remarkable as its eventual decay, however, is the long period (~50 days) during which sensitive hearing is preserved. We probed the molecular bases of this homeostatic preservation. The specific environmental conditions of our ageing cohorts (see methods for details) meant that antennal stimulations occurring during the flies' life course were almost exclusively caused by the animals' own locomotion, thereby approximating the minimal noise floor possible for freely moving, intact flies. Our study thus explored the gene regulatory network of auditory homeostasis in acoustically unchallenged ears.

Across taxa, ears are delicate mechano-electrical converters. Their operation can be conceptually divided in a *passive* and an *active* component. Both with regard to its natural life course and the effects of our transgenic manipulations the steady-state stiffness, K_{steady} (a good indicator of the passive oscillator [16]) - remained one of the most stable parameters of auditory function (Fig. 1d and Fig. 4d), suggesting that the causes for the functional decline emerge from the active system. The *active* oscillator of the fly's ear emanates from its auditory transducer modules, i.e. mechanosensory ion channels that act in series with – and receive feedback from [17] – probably dynein-based motor proteins [27]. This functional design explains vast parts of the functional performance of the *Drosophila* ear [17]; its quantitative modelling also allows for extracting vital parameters of auditory function, such as the amount of energy that auditory neurons inject into the hearing process or the number – and molecular properties – of transducer channels they harbour.

Quantitatively, the hearing loss observed in flies older than 50 days is best described as a loss of power gain (Fig 1c), i.e. a loss of the active, transducer-based process by which auditory neurons amplify sound-induced motions of the antennal sound receiver. Comparing the rather sharp drop of the flies' auditory life span to their survival rates reveals a close alignment of the two time courses (Fig. 6). This suggests that the - metabolically costly - operations of the homeostatic network have evolved to maintain function up to the expected lifespan but not beyond. Such behaviour has been predicted by the 'disposable soma' theory of ageing [47,48], which postulates that an organism's investment in somatic maintenance will not exceed its reproductive period [48]; the dissociation between healthspan and lifespan observed in today's

human societies, and evidenced not least by ARHL, lies at the heart of these evolutionary relations.

The flies' age-related loss of auditory power gain is accompanied by a gradual loss of nerve response (CAP amplitudes), which decline steadily from day 25 already, in both males and females, potentially indicating a progressive neuropathy (Fig. 1d). This shows that ageing occurs on various levels of auditory function, including transduction, motor-based feedback amplification and signal transformation into action potential responses. Auditory transducers, however, also display a remarkable resilience throughout life; the characteristic nonlinear signatures they introduce into sound receiver mechanics (gating compliances) stay broadly constant up to the age of 70 days (Fig. 1d). First quantitative gating spring model analyses also hint at a possible homeostatic mechanism for this constancy: In both males and females, and across ages, transducer channel numbers were found to be inversely correlated with their respective single channel gating forces. When transducer numbers decrease with age, their single channel gating forces increase, thereby stabilizing the nonlinear mechanics of the sound receiver across the auditory life course (Supplementary Fig. 3). This homeostatic stabilization of receiver nonlinearity is particularly significant, as all changes in receiver mechanics will affect all neurons and thereby global JO function. In order to understand these, and other, homeostatic mechanisms we explored the transcriptional network that mediates them.

We found that 16,243 genes are expressed in the 2nd antennal segment, which harbours the fly's inner ear (JO); 5,855 out of these change their expression in at least one of the pair-wise age comparisons. Four transcription factors emerged from our bioinformatical analysis as key regulators of the age-variable auditory transcriptome, all of which are conserved in the human genome; these are Onecut, Worniu, Optix and Amos.

Onecut is a transcription factor known to be involved in photoreceptor differentiation in flies [49] and retinal ganglion cell development in mice, where it cooperates with Pou4f2 (*acj6*) and Atoh7 (closest fly orthologues: *ato, amos*) [50]. We here report an essential role for Onecut in fly hearing or - more precisely – in the homeostatic maintenance of fly hearing. An adult-specific knockdown (KD) of the *onecut* gene across JO neurons affects all levels of auditory system function and leads to deafness. The *onecut* KD phenotype includes near complete losses of auditory (i) transducer gating, (ii) amplification and (iii) nerve responses, as well as (iv) a loss of sound-evoked behaviour. A first probing of possible Onecut targets through qPCR in *onecut* KD flies (Fig. 4f) might reveal one possible mechanism of action, which is the direct transcriptional regulation of the two interdependent TRPV channels Nan and Iav. Nan/Iav are thought to form a heterodimeric ion channel specifically in chordotonal neurons. Both genetic

[44,45] and pharmacological [51] ablations of Nan/Iav channels have been shown to eliminate chordotonal mechanosensory function. After an adult-specific knockdown of *onecut*, JO expression levels of both *nan* and *iav* showed a dramatic decline. This downregulation coincided with a near complete abolition of the gating compliances associated with sound-sensitive neurons, indicating a failure of auditory transduction. A total loss of transducer function would also be sufficient to explain the effects on auditory amplification and nerve responses observed further downstream the auditory signalling chain. Intriguingly, *onecut* was also predicted to be upstream of the kinesin-dependent machinery for anterograde transport in chordotonal cilia (Supplementary Fig. 7a). The observed total absence of Iav expression in JO after *onecut* KD (Supplementary Fig. 7b) could thus be the combined result of a reduced transcription (see Fig. 5a) and a defective ciliary transport, which requires kinesin activity. Interestingly, both Nan/Iav [44,45,52], as well as NompC [53,54], have previously been proposed as auditory transducer components in *Drosophila*. Further studies also demonstrated beyond doubt that NompC contains all elements required to form a bona-fide mechanotransducer channel [55,56]. In contrast to *nan*/*iav*, however, *nompC* transcript levels in JO remained unchanged after *onecut* KD.

worniu (*wor*) is a zinc finger transcription factor that belongs to the Snail family. We here demonstrate that adult-specific down-regulation of *wor* enhances auditory amplification and sharpens auditory tuning. These effects are sustained up until 30 days of downregulation (at 30°C) - when the ears of control flies already show a near complete loss of power gain - suggesting that knockdown of *worniu* can protect distinct aspects of auditory function from their age-dependent decline. Genes previously reported to be upregulated in *wor* mutants included cadherins and trafficking proteins, e.g. Rabs [57]; our bioinformatics prediction also support a role of wor in the regulation of the cellular trafficking machinery (Supplementary Fig. 2). In JO, the adult-specific KD of *wor* had virtually no effect on auditory transducer gating or the transformation of antennal motion into nerve responses. Auditory amplification and tuning sharpness, however, were significantly enhanced in *wor* KD flies; both of these parameters are linked to the dynein-based motor machinery that acts in series with the auditory transducer channels. Consistent with these mechanistic considerations, qPCR analyses of the JOs of *wor* KD flies showed a downregulation of Dhc98D; neither *nompC*, *nan* nor *iav* levels were affected.

Optix belongs to the sine oculis homeobox (SIX) family of transcription factors and is required for eye formation [58]. The adult-specific knockdown of *Optix* in JO neurons leads to an increase in the receiver's power gain and a shift of its best frequencies to lower values, both indicative

of more active system. qPCR analyses showed that these changes in auditory activity coincided with an upregulation of *nompC*. These relations are consistent with the reported roles of NompC in auditory amplification [46]. Auditory transducer gating, however, was not affected; both numbers and single channel gating forces of sensitive auditory transducers were identical between the ears of Optix KDs and control flies. Also, CAP responses to small antennal displacements (as caused by auditory stimuli) were unchanged. CAP responses to larger displacements (as caused by non-auditory stimuli), in contrast, were decreased as compared to controls. This suggests a more complex role of Optix in the homeostatic regulation of auditory, as well as non-auditory populations of JO neurons.

amos is a proneural gene from the family of basic-helix-loop-helix (bHLH) transcription factors. bHLH transcription factors also include *ato*, which specifies chordotonal organs [20,59], R8 photoreceptor precursors [59,60], and a subset of olfactory sense organs [61]. *amos* specifies two other subsets of olfactory sense organs and a mechanosensory subset of larval bipolar dendritic neurons [62,63]. *Ato* and *amos* share a high sequence similarity in their bHLH domains (73% amino acid identity) and their basic - DNA-binding - regions are identical. Maung and Jarman showed that *amos* is capable to rescue eye development independent of *ato* [64]. Weinberger et al. showed that the coding sequence of *amos*, when used to replace the coding sequence of *ato*, is sufficient to produce a fully functional *Drosophila* ear, the performance of which is statistically identical to the native, *ato*-induced organ with respect to all quantitative parameters also used in this study [23]. While *amos* was found to be expressed in adult JOs, no such expression was found for *ato*. Consistent with this finding, an adult-specific knock-down (KD) of *ato* did not have any significant effect on fly hearing (Supplementary Table 6). This does, however, not exclude the possibility that perturbing *ato* expression developmentally might affect the ear's homeostatic resilience and lead to dysfunction later in life, as has been shown for Atoh1 in the mouse cochlea [65].

The KD of *amos*, in contrast, produces an accelerated hearing loss phenotype that is characterised by a loss of power gain and tuning sharpness. Interestingly though, best frequencies of *amos* KD receivers do not move towards the passive system but instead show a small - but significant - move in the opposite direction, indicating a larger independence between fundamental parameters of *Drosophila* hearing than appreciated by current models [17,66]. *amos* KD also leads to a loss of nerve responses in high-threshold units of JO and a homeostatic reorganization of sensitive transducer channels, characterised by a slight decrease in single channel gating forces and a slight increase in channel number (Fig. 4d). Consistent with bioinformatical predictions, qPCR analyses of JOs of *amos* KD flies showed

significantly reduced expression levels for the here newly described auditory dynein Dhc98D but no effects on the three auditory TRP channels tested (nompC, nan, iav).

Interestingly, all four master regulators are predicted to act upstream of phototransduction genes (Fig. 2b), including visual opsins, which have been previously linked to *Drosophila* auditory function [28] and ciliary maintenance [67] and are also upregulated during auditory ageing (Fig. 2a). This indicates a substantial regulatory overlap between the auditory and the visual system, which might not be restricted to *Drosophila* as a brief comparison with the respective mammalian transcriptomes suggests (see Supplementary Table 5 for details). 78% of the predicted regulators (29 human orthologues of 37 *Drosophila* TFs) were previously shown to be expressed in the human retina and associated with age-related macular degeneration (AMD) [68]. Shared homeostasis genes may well be a molecular substrate for auditory/visual co-morbidities (e.g. ARHL + AMD).

The human orthologues of 29 predicted TFs, finally, were found to be expressed in the adult human inner ear (see Supplementary Table 5 for details) [69], including close orthologues of *amos* (ATOH8), *Optix* (SIX1, SIX2 and SIX4), and orthologues of *wor* (SNAI1, SNAI2, SNAI3). The human orthologue of *Drosophila sox14* (SOX4) has also recently been identified in a GWAS of age-related hearing loss [15]. Down-regulation of *sox14* in flies results in a hearing loss phenotype (see Supplementary Table 6). Most of the other predicted TFs, which showed functional relevance in our study are conserved, and expressed, in the human inner ear, e.g. *aop* (ETV5), *ara* (IRX1-3), *lola* (ZBTB20), *pnr* (GATA2, GATA3), *run* (RUNX1, RUNX2), *ct* (CUX1, CUX2), and *Stat92E* (STAT1-6); or in the mouse inner ear, *onecut* (Onecut3), *Optix* (Six1-6), *Pph13* (Alx3), *wor (*Snai1, Snai2), *amos* (Atoh1, Neurod1, Neurod6).

These findings reinforce the narrative of a transcriptional homeostatic machinery, which is conserved between flies and humans and required to maintain not only hearing but also vision.

Our study has identified novel master regulators of auditory maintenance, some of which work as bidirectional homeostatic actuators within the fly's auditory neurons. If the regulator's upregulation, e.g., results in an improvement of a specific auditory function, then its downregulation leads to a worsening (*amos*), or vice versa (*Optix*).

It seems obvious that homeostatic mechanisms will not be restricted to the transcriptomic level but extend further to the auditory proteome. In fact, the prominence of age-variable heat-shock proteins and kinases in our own transcriptomic data clearly points to the relevance of post-translational, e.g. proteostatic, mechanisms. The vital role proteostasis plays in general ageing

445 [70] and hearing in particular [71,72] is becoming increasingly recognised and also merits further
446 exploration in the *Drosophila* ear.

447 Future studies will apply the powerful combination of transcriptome profiling and computational
448 analyses, which has already contributed to advancing our knowledge of the complex
449 regulatory networks underlying hearing and deafness [73] and will also shed more light on the
450 downstream targets of the here identified transcription factors and their specific roles in
451 auditory homeostasis. Some key conclusions, however, can be drawn already. All four master
452 regulators that emerged from our screen are evolutionary conserved; they either form key
453 regulators of specific sensory (or neural) tissues or constitute paralogs of such regulators; their
454 predicted (and in part validated) regulons, however, do not comprise of classic developmental
455 genes (such as proliferation, apoptosis) but rather of known effector genes for specific auditory
456 functions, e.g. ion channels and motor proteins. This suggests a scenario where
457 developmental and homeostatic functions are divided between pairs (or groups) of paralogs.
458 Examples for such pairs from our study would be *ato*/*amos* or *ct*/*onecut*. Sometimes, as is the
459 case for the proneural master gene *ato*, the homeostatic roles seem to have been fully
460 transferred to a paralog (*amos*). The 19th century recapitulation theory (or *biogenetic law*) [74]
461 proposed that ontogeny recapitulates phylogeny to explain the phenotypic similarities between
462 early developmental stages of evolutionarily younger species (e.g. mammals) and more adult
463 stages of evolutionarily older species (e.g. fish). In analogy, one might propose that an organ's
464 homeostatic maintenance (organostasis) partly recapitulates its development
465 (organogenesis). The original biogenetic law has meanwhile been refined, and rewritten, as
466 hourglass model of evolution, which posits that for every animal there is a specific phylotypic
467 stage during which it most closely resembles other species [75]. This resemblance also extends
468 to the molecular level: Expression patterns of key developmental genes are most conserved
469 between species during this phylotypic (or also organotypic) phase [76]. Together with the
470 reported high conversation of binding specificities between fly and human TF orthologues [77],
471 an hourglass model of sensory homeostasis might indeed be a valuable guide for the
472 translational route from *Drosophila* ear to human cochlea. This could also have implications
473 for the design of gene-therapeutic trials to reverse human hearing loss, which currently
474 concentrate on key developmental genes - such as e.g. ATOH1. ATOH1's 'next of kin' – such
475 as e.g. ATOH7, ATOH8 or NEUROD1 – might be worth having a look at.

476

477

478

479

Materials and Methods

Rearing conditions for auditory ageing

Unless otherwise specified, flies were raised on standard medium in incubators maintained at 25°C and 60% relative humidity (RH), with a 12 hr:12 hr light:dark cycle. Virgin female and male flies were collected on the day of eclosion using CO_2 sedation and allowed to age in separate vials at 25°C for 1, 5, 10, 25, 50, 60 and 70 days – all biomechanical and electrophysiological experiments were conducted at room temperature (21°C - 22°C) . Adult-specific RNAi knock-down mutants (whose larvae and pupae were kept at 18°C in order to repress the Gal4-mediated transcriptional activation via a $Gal80^{ts}$ repressor) were collected on the day of eclosion and transferred to 30°C (for maximal activation of the Gal4/UAS expression system), 60% RH and kept at 12 hr:12 hr light:dark cycles for 2 weeks prior to the experiments. Flies were raised under conditions, which formed a near zero-noise environment for their particle velocity sensitive antennal receivers. Conditions included: (i) separate housing of virgin males and females at low densities (20-25 flies per vial), in (ii) environmentally controlled incubators, with (iii) regular transfer to fresh medium (twice a week) and at ambient sound levels below the hearing threshold. Antennal stimulation across the flies' life course was thus occurring almost exclusively as a result of the animals' own locomotion. As a result of the low density of their housing and the abundance of food no aggressive interactions were observed.

Life span measurements

Three independent cohorts of male Canton-S flies were set up in parallel. The density of flies per vial (25) was kept constant, the flies were transferred to a fresh medium every 3 days, and the number of dead flies was counted. The flies were kept at 60% RH and kept at a 12 hr:12 hr light:dark cycles for approx. 80 days. Rearing conditions were identical to the ones used for the auditory ageing experiments described above.

Fly stocks used

To assess the natural life course of hearing in *Drosophila* the following lines were used as wildtype references: Canton-S line (Bloomington), Canton-S (Goodwin lab), Canton-S (Kamikouchi lab), Oregon-R.

To probe the expression of predicted transcription factors the following lines used: Fly-TransgeneOme (fTRG) sGFP tagged lines from VDRC[78] for *amos*, *onecut* and *Optix* (*optix:GFP 318371/10042*), *wor*-Gal4 (kindly provided by A. Carmena).

elav-Gal4; UAS-RFP-nls/+; Mi{PT-GFSTF.0}alphaTub85E[MI08426-GFSTF.0]/+ was used to monitor JO neurons across the flies' lifespan.

y[1]w[*]; tub-Gal80ts; NP0761 was used for adult-specific downregulation (via RNAi knock-down) or upregulation (via overexpression) of target genes across all JO neurons.

RNAi lines were obtained from the Bloomington *Drosophila* Stock Centre (BDSC) and Vienna *Drosophila* Research Centre (VDRC). Attp2 and attp40 served as control lines for the TRIP collection and VDRC 6000 was used as control for the KK lines.

y[1] sc[*] v[1]; P{y[+t7.7] v[+t1.8]=TRiP.HMS01438}attP2	onecut RNAi
y[1] v[1]; P{y[+t7.7] v[+t1.8]=TRiP.JF02254}attP2	lola RNAi
y[1] v[1]; P{y[+t7.7] v[+t1.8]=TRiP.HM05094}attP2	srp RNAi
y[1] v[1]; P{y[+t7.7] v[+t1.8]=TRiP.JF02518}attP2	Rfx RNAi
y[1] sc[*] v[1]; P{y[+t7.7] v[+t1.8]=TRiP.HMS00924}attP2	ct RNAi
y[1] sc[*] v[1]; P{y[+t7.7] v[+t1.8]=TRiP.HMS01186}attP2/TM3, Sb[1]	run RNAi
y[1] sc[*] v[1]; P{y[+t7.7] v[+t1.8]=TRiP.HMS01430}attP2	ato RNAi
y[1] sc[*] v[1]; P{y[+t7.7] v[+t1.8]=TRiP.HMS01256}attP2	aop RNAi
y[1] v[1]; P{y[+t7.7] v[+t1.8]=TRiP.HMC03993}attP2	Optix RNAi
y[1] sc[*] v[1]; P{y[+t7.7] v[+t1.8]=TRiP.HMC04197}attP40	Tbp RNAi
y[1] sc[*] v[1]; P{y[+t7.7] v[+t1.8]=TRiP.HMS01082}attP2	pnr RNAi
y[1] v[1]; P{y[+t7.7] v[+t1.8]=TRiP.HMC03988}attP2	gl RNAi
y[1] sc[*] v[1]; P{y[+t7.7] v[+t1.8]=TRiP.HMS00103}attP2	sox14 RNAi
y[1] sc[*] v[1]; P{y[+t7.7] v[+t1.8]=TRiP.HMC05094}attP40	amos RNAi
y[1] v[1]; P{y[+t7.7] v[+t1.8]=TRiP.HMS00035}attP2	Stat92E RNAi
y[1] v[1]; P{y[+t7.7] v[+t1.8]=TRiP.JF02233}attP2	Aef1 RNAi
VDRC 110594 KK line	Pph13 RNAi
VDRC 105362 KK line	wor RNAi

VDRC 101903 KK line ara RNAi

y[1]w[*]; P{UAS-Optix.S}1

w[*]; P{UAS-amos.G}5

w[*]; P{UAS-ato.J}8/TM3, Sb1

w[*]; P{UAS-wor} [kindly provided by J.Knoblich]

y[1] sc[*] v[1] sev[21]; P{y[+t7.7] v[+t1.8]=TRiP.HMC06494}attP40 Dhc98D RNAi

Immunostainings of JO

To probe the expression of predicted transcription factors, the following lines were used: Fly-TransgeneOme (fTRG) sGFP tagged lines from VDRC[78] for *amos*, *onecut* and *Optix* (*optix:GFP 318371/10042*), *wor*-Gal4 (kindly provided by A. Carmena).

Fixation and immunostainings followed standard procedures. Briefly, 10 days old adult female heads were dissected in PBS, fixed with a 4% formaldehyde solution (in PBT) for one hour while rotating at room temperature (RT); three heads were placed exposing the antennae into silicon blocks filled previously with hot gelatin-albumin mixture. Silicone blocks were then quickly cooled down at 4°C for 10 minutes and incubated with 6% formaldehyde solution overnight at 4°C. Thereafter, silicone blocks were extracted and incubated further with Methanol for 10 min at RT, before being washed with PBS for 30 min at RT. 30 µm vibratome sections were cut using a vibratome (Ci 5100mz, Campden Instruments) and antennae sections collected in PBT (PBS with 0.3% Triton X-100) and afterwards washed three times for 15 min at RT. After blocking for 1 hr at RT (blocking solution: PBS with 1% Triton X-100, 2% BSA, 5% normal goat serum), samples were incubated with primary antibodies in blocking solution overnight at 4°C, then washed again three times in PBT and incubated with secondary antibodies diluted in blocking solution for 2 hr at RT. Samples were then washed again three times in PBT and, finally, briefly washed in PBS before mounting. Primary antibodies used in this study are:

Rb anti-GFP 1:1000 (Life Technologies), Rat anti-elav 1:250 (Hybridoma Bank), Goat anti-HRP::Cy3 1:500 (Jackson ImmunoResearch). Secondary antibodies conjugated with Alexa 488, and Alexa 633 (Life Technologies) were used at 1:500. All samples were mounted in Dabco (Molecular Probes, H-1200). Images were acquired with a LSM 510 Zeiss confocal microscope with a Plan-Neofluar 40x/1.3 Oil objective. Z-stacks (optical slice thickness: 1µm)

were taken to image throughout Johnston's organ (JO). Images were assembled and analysed in ImageJ (Fiji).

Immunostainings of pharate adult JOs

The RNAi line for *onecut* was crossed to iav-Gal4, iav::GFP. Crosses were kept at 18 °C until the 3rd instar larval stage and then shifted to 25 °C. The antennae of pharate adult flies (post-metamorphosis but pre-eclosion) were fixed in 3.7% formaldehyde for 30min and blocked for >2h in 3% BSA at RT. Primary antibodies were added for 48h and secondary antibodies overnight at 4 °C. Alexa568-conjugated phalloidin (Molecular Probes, 1:2000) was added for 45min at RT following incubation with secondary antibody. Rb anti-GFP (Invitrogen), anti-RbAlexa488 (Molecular Probes) were used at 1:500.

Neuron counts

Flies of genotype *elav*-Gal4; UAS-RFP-nls/+; Mi{PT-GFSTF.0}alphaTub85E[MI08426-GFSTF.0]/+ were aged at 25°C. Fly antennae of day1, day5, day25 and day 50 flies were dissected in PBS, such that left and right antennae remained attached to the cuticle, and that the third antennal segment and the associated arista remained intact. Antennae were then briefly fixed for 10 minutes in 4% formaldehyde in PBS, washed three times in PBT and finally mounted in glycerol. Fly JO-s were imaged with an LSM 510 Zeiss confocal microscope with a Plan-Neofluar 40x/1.3 Oil objective. Z-stacks (optical slice thickness: 1μm, 80 slices in total) were taken to image throughout Johnston's organ (JO). Images were processed and unspecific background removed using the FluoRender programme. Single Z-stacks were processed in ImageJ. The Eve programme (based on the algorithm from Shimada et al. 2005 and kindly provided by Kei Ito)[79] was used to count neurons automatically (XY:Z ratio was set depending on the number of the stacks), neuron radius was set to 4 and Bending 1 at 300 cells was used as a cut-off. Processed images were saved as new files (including cell count information) and result files were produced. Number of cells was corrected manually by using the ImageJ cell counter plugin.

RNA sequencing

Virgin male and female Canton-S flies of different ages (days 1, 5, 10, 25, and 50) were anesthetised on ice, their second antennal segments dissected and collected in Lysis Buffer (containing 1% β-mercaptoethanol, as provided in the Qiagen RNeasy Mini Kit). As soon as dissections were completed for a given time point, samples were frozen at -80°C. When

enough samples were collected, RNA was extracted according to the Qiagen RNeasy Mini Kit protocol.

Reverse transcription and pre-amplification were carried out with the SMART-Seq v4 Ultra Low Input RNA Kit for Sequencing (Clontech). All samples were quality controlled and cDNA concentrations measured with an Agilent BioAnalyzer 2100. Sample libraries were prepared with a Nextera XT DNA Library Preparation kit (Illumina). Thereafter, paired-end 75bp reads were sequenced on an Illumina NextSeq 500 platform.

The RNAseq .fastq files were aligned in the Partek Flow software to the most recent version of the *Drosophila* genome (dm6) obtained from the Berkeley *Drosophila* Genome Project at UCSC.

In order to generate raw sequence counts, .bam files created in Partek software were processed in HTSeq. These counts were then used in DESeq2 in R/Bioconductor to measure differential expression across genes and for conducting ANOVA statistical analyses of each comparison. Further data filtering took place to reduce the maximum false discovery rate (FDR) to 10% limiting the expression fold change threshold to ±1.5x.

Quantitative PCR (qPCR)

Flies of different genotypes were collected and frozen immediately with liquid nitrogen and then kept at -80°C. After 50 flies were collected they were vortexed and second antennal segments were collected (100 antennae) in Lysis Buffer containing 1% β-mercaptoethanol (as part of the Qiagen RNeasy Mini Kit). In accordance with the Qiagen RNeasy Mini Kit protocol, RNA was extracted immediately and RNA samples were then kept at -80°C.

Reverse transcription was carried out with the High Capacity RNA to cDNA kit (Applied Biosystems) following the manufacturer's protocol.

In order to proceed to pre-amplification with TaqMan PreAmp Master Mix Kit, a "pooled assay" of Taqman primers was prepared (containing probes for the target genes of interest, i.e. *nompC*, *nan*, *iav*, *Dhc98D*). TaqMan probes of interest were mixed together and diluted 1:100 in TE buffer. The pre-amplification procedure followed the manufacturer's protocol. The pre-amplified cDNA was diluted 1:20 in RNAse and DNAse-free water and the qPCR was performed in the immediate aftermath. qPCR assays were run on a Step One Plus ABI machine. Prior to the reaction, the 96 well plate set up was designed with help of the Step One Plus software. Three negative controls were run per target as well as three replicates for each sample and each target. *SdhA* was chosen as endogenous control as one of the housekeeping genes that has the most stable expression at different ages [80].Reactions were prepared according to the TaqMan Gene Expression Assay protocol.

Cycle threshold (Ct) values were extracted from the Step One Plus Software data analysis. The ΔΔCt and relative quantification were calculated in Excel as follows:

$$\Delta Ct = \left(Ct_{gene\ x\ control} - Ct_{endogenous\ control}\right)$$

$$\Delta\Delta Ct = \Delta Ct - \left(Ct_{gene\ x\ knockdown} - Ct_{endogenous\ control}\right)$$

$$RQ = 2^{-\Delta\Delta Ct}$$

The three RQ values were averaged for each biological replicate and standard deviations generated in Excel. At least three biological replicates were performed for each experiment. Statistical were performed in SigmaPlot.

Bioinformatical analysis in iRegulon

The iRegulon plug-in [41] was used in the Cytoscape software to predict transcription factors/regulators based on their binding motifs. A list of genes of interest was submitted and predicted transcription factors were then selected according to their normalised enrichment scores (NES) for a particular motif, or group of motifs, within the list originally submitted to iRegulon.

Gene ontology analysis - GORILLA

The online interface GOrilla (**G**ene **O**ntology en**RI**chment ana**L**ysis and visua**L**iz**A**tion tool) was used to classify genes of interest according to their gene ontology [37,38]

Functional classifications were generated for biological processes and molecular functions. Enrichment scores were calculated:

Enrichment = (*b*/n) / (*B*/*N*),

where *b* is the number of genes in the intersection, *n* the number of genes in the target set, *B* the total number of genes associated with a specific GO term and *N* the total number of genes.

Preparation of gene lists for submission to iRegulon and transcription factor (TF) selection:

Submission round I - The identified 5,855 age-variable genes were submitted to the **G**ene **O**ntology en**RI**chment ana**L**ysis and visualization (GOrilla) tool. Gene sets from four hearing-relevant gene ontological categories ([i] trafficking genes, [ii] structural genes, [iii] dynein motor proteins and [iv] receptors, see Suppl. Figure 2) were then submitted to iRegulon to

predict their upstream regulatory genes (TFs) based on binding motif enrichment scores (cut-off: threshold 2.5, Rank threshold: 5,000). This generated a first list of candidate TFs.

Submission round II – The most highly expressed age-variable genes (>10,000 reads) were submitted to iRegulon (same cut-off thresholds as above). This generated a second list of candidate TFs.

Submission round III – Genes showing the greatest age-variability (down- or up-regulated by at least 4-times in at least one age comparison) were submitted to iRegulon (same cut-off thresholds as above). This generated a third list of candidate TFs.

In a final step, all candidate TFs (from I-III above) were filtered further to choose those subjected to functional testing: (i) suitable transcription factors had to show expression in JO, i.e. they had to be part of the 16,243 genes identified in our RNA-Seq (see Suppl Table 2). This brought the total number of TFs to 37 (see Suppl. Table 5); (ii) a random (~50%) selection of these TFs (19 in total) was then chosen for functional biomechanical tests (fluctuation analyses) in RNAi knockdown lines. The four TFs showing the strongest phenotypes (Onecut, Amos, Optix, Worniu) were then chosen for in-depth functional characterisation.

JO functional analyses

For all analyses of JO function, flies were mounted as described previously [16]. Briefly, flies were attached, ventrum-down, to the head of a Teflon rod using blue light-cured dental glue. The second segment of the antenna under investigation was glued down to prevent non-auditory background movements. The antenna not under investigation was glued down in its entirety, thereby completely abolishing any sound-induced motion and interference with the contralateral recordings. An active vibration isolation table (model 63-564; TMC, USA) was used. After mounting, flies were oriented such that the antennal arista was perpendicular to the beam of a laser Vibrometer (PSV-400; Polytec, Germany) and free fluctuation recordings could be taken. To allow for ultrafast, contact-free, non-loading stimulation, electrostatic actuation (EA) was used. EA is conducted via two external actuators positioned close to the arista (for details see Albert et al., 2007 [16] and Effertz et al., 2012 [53]).Two electrodes were inserted into the fly – a charging electrode was placed into the thorax so that the animal's electrostatic potential could be raised to -20 V against ground, and a recording electrode for measuring mechanically evoked compound action potentials (CAPs) was introduced close to the base of the antenna under investigation. The charging electrode also served as reference electrode for the CAP recordings.

Arista displacements were measured at the arista's tip using a PSV-400 LDV with an OFV-70 close up unit (70 mm focal length) and a DD-500 displacement decoder. The displacement output was digitized at a rate of 100 kHz using a CED Power 1401 mk II A/D converter and loaded into the Spike 2 software (both Cambridge Electronic Design Ltd., Cambridge, England). Free (i.e. unstimulated) fluctuations of the arista were recorded both before and after the experiment to monitor the physiological integrity of the antennal ear. Free fluctuations were then analysed in SigmaPlot (Systat Software, Inc), where simple harmonic oscillator models were fitted to the velocity data as previously described [18,23] (see also Supplementary Fig. 6). Median fits (calculated from the median values of individual fits) are shown as line plots (Figs. 1c, 4a, 5b; Supplementary Figs. 5 and 6b). Only those flies, which maintained a stable antennal function throughout the experiment (maximally allowed change of best frequencies: 20%) were analysed.

Approximate equivalence of hearing parameters between *Drosophila* and humans: analyses of the fly's auditory mechanics (free fluctuation and gating compliance analyses) probe for hearing loss that originates within the chordotonal transducer sites proper (human equivalent: stereociliary bundles of hair cells). Calculated power gain values quantify hearing sensitivity; the maximal gain of the fly's auditory amplifier is ~20-30dB (the gain of its functional equivalent, the human cochlear amplifier, is ~50-60dB). CAP responses roughly correspond to human ABR measurements. Together, the used set of measurements allows for allocating the likely cause of the observed hearing impairments (loss of transduction, loss of amplification or neuropathy). Please note that *Drosophila* chordotonal neurons – in contrast to human hair cells - are primary neurons, which directly send axon potentials to the brain.

Tests of sound-evoked behaviour

Drosophila melanogaster males increase locomotor activity in response to a playback of courtship songs [31]. We exploited this phenomenon to test hearing across the *Drosophila* life course. To conduct measurements, flies were housed in 5x65mm Pyrex glass tubes. One end of the tube was sealed with an acoustically transparent mesh, the other end contained food consisting of 5% sucrose and 2% agar medium covering ~ ¼ of the tube. Glass tubes were then loaded into high-resolution *Drosophila* activity monitors (MB5; Trikinetics, Walham, USA). MB5 monitors harbour 17 independent infrared (IR) beams bisecting each tube at 3mm intervals, allowing for a high-fidelity recording of the flies' activity. Detectors were set to count all beam breaks occurring within one minute for the duration of each experiment. Activity counts were registered independently at each beam position within a tube; all beam breaks,

735 irrespective of beam position, were then pooled. This procedure allowed for calculating the
736 total activity of all flies in that tube. To maximise data collection, three MB5 monitors were
737 stacked together forming a grid allowing to record from 36 tubes (totalling 108 flies)
738 simultaneously over the course of a single experiment. The MB5 activity monitors were placed
739 centrally in front of a 381mm wide bass speaker (Eminence Delta 15, 400W, 8 ohm) with the
740 tubes' acoustically transparent mesh facing the speaker at a distance of ~60mm from the
741 speaker membrane. The speaker was connected to an amplifier (Prosound 1600W). To avoid
742 interference from non-air-borne vibrations, the MB5 monitors – but not the speaker - were
743 placed on a vibration isolation table. Sound stimuli were adjusted to reach peak amplitudes of
744 90 dB SPL at the middle of the monitor tubes. Courtship stimuli played at these intensities are
745 known to elicit reproducible behavioural responses in males [81]. The sound stimulus (played,
746 and controlled from the Spike2 software) consisted of a 'master pulse' that was repeated to
747 form 2s long trains with 40ms interpulse intervals (IPIs). The master pulse was generated by
748 averaging previously recorded original courtship song pulses (~1000 pulses from 10
749 Drosophila melanogaster males). Each pulse train was followed by a 2s long silence; this
750 elementary kernel was played continuously for 15 minutes at the beginning of every hour. The
751 15 min of sound stimulation were played in loop with 45 min of silence for an entire circadian
752 day (24h at a 12-hour light, 12-hour dark cycle). Responses for each hour were then collapsed
753 into a single median response to cancel out any circadian variations of responsiveness.

754 Activity displayed during *stimulus presentation* was determined by the sum of all activity
755 displayed during the first 15 minutes of every hour (i.e. during the phase of sound stimulation)
756 and averaged over the whole experimental day. *Baseline activity* was determined by the sum
757 of all activity displayed during the last 15 minutes of every hour (i.e. during the silent phase
758 directly preceding the next stimulus phase) and also averaged over the whole experimental
759 day.

760 The room, in which the recordings took place was held at a constant 25˚C temperature (@
761 ~40% RH) and followed a 12-hour light, 12-hour dark cycle, which was kept consistent with
762 the flies' entrainment regime prior to experiment start. Exposure to courtship sound is known
763 to induce male flies to also produce mating songs. To prevent these stimulus-induced mating
764 songs from interfering with the sound stimulus, experimental flies were anaesthetized using
765 CO_2 and their wings clipped 2-4 days prior to the initiation of the experiment. At least 2/3 of
766 the wing was removed using microdissection scissors. After allowing time for healing post
767 procedure, the flies were again CO_2-anesthetized and transferred into the glass tubes before
768 being placed into the MB5 monitors. For each experiment, flies were exposed to the sound
769 stimulus as soon as they were placed into the monitors; however, only data recorded from the
770 first light transition on was used for analysis. This allowed flies to have ~12hr to adapt to the

stimulus, the new environment and to recover from after-effects of CO2 exposure. After this equilibration stage, data was collected for 48 hours.

Data Availability

The datasets generated and analysed during the current study are available in the the Gene Expression Omnibus (GEO) of the National Center for Biotechnology Information (NCBI); accession code: GSE148023
https://www.ncbi.nlm.nih.gov/geo/query/acc.cgi?acc=GSE148023

Acknowledgements

We'd like to thank Ana Carmena de la Cruz (Instituto de Neurociencias, Alicante) and Jürgen Knoblich (IMBA, Vienna) for providing reagents. We are also grateful for fly ageing advice from Linda Partridge and Nathaniel Woodling (UCL Institute of Healthy Ageing, London). We also thank Stefan Németh (SCIMED Illustrations, Vienna) for help with Figure 1a. This work received funding from the Biotechnology and Biological Sciences Research Council (BBSRC), UK (BB/M008533/1 to JTA, AJ and JEG) and BBSRC 16Alert equipment award BB/R000549/1 to JEG, JTA et al.) and from the European Research Council (ERC) under the Horizon 2020 research and innovation programme (Grant agreement Nos 648709 and 862216, both to JTA).

Figure legends

Figure 1. *Drosophila* Hearing across the life course

(a) Schematic representation of Johnston's Organ (JO), a chordotonal organ located in the 2nd antennal segment. JO harbours the mechanosensory units (scolopidia) that mediate the sensation of sound in *Drosophila*. Sound waves act on the feathery arista, forcing the 3rd antennal segment to rotate about its longitudinal axis, thereby stretch-activating specialised mechanosensory ion channels (Nan, Iav, NompC) in the scolopidial neurons.

(b) Sound-evoked activity (shown in light blue, male locomotor responses to courtship song, seen in 10-day and 50-day old flies ($p<0.001$ in both, paired t-test) are abolished in 60-day old flies. Baseline activity levels (shown in grey, male locomotor activity when not stimulated) are not significantly different between 10 and 60 day old flies. [$p=0.487$, t-test; sample sizes: n(day 10)=12, n(day 50)=10, n(day 60)=14].

(c) Power Spectral Densities of unstimulated antennal sound receivers betray age-related decline of hearing in both males (left, shades of blue) and females (right, shades of red). Preceded by homeostatic oscillations around their baseline values, all principal parameters of hearing (shown in right-hand panels for both sexes) indicate a loss of hearing from day ~50 onwards: the receiver's best frequency starts rising towards the level of the passive system, the auditory energy gain drops to near zero and tuning sharpness falls to values around ~1. [sample sizes males: n(day 1)=18, n(day 5)=13, n(day 10)=6; n(day 25)=19, n(day 50)=16), n(day 60)=11, n(day 70)=18; sample sizes females: n(day 1)=17, n(day 5)=8, n(day 10)= 4; n(day 25)=17, n(day 50)=20), n(day 60)=12, n(day 70)=17]

(d) Mechanical and electrophysiological responses to force steps allowed for probing JO mechanotransducer function across the auditory life course in male (left, blue) and female (right, red) flies. Mechanical integrity of auditory transducers was quantified by fitting gating spring models to the antennal receiver's dynamic stiffness (slope stiffness) as a function of its peak displacement (see ref. [16] for details). Electrophysiological function was assessed by recording compound action potential (CAP) responses from the antennal nerve. CAP responses showed an identical pattern across the life course in both males and females: CAP response magnitudes substantially increased from day 1 to day 25, then monotonously declined from day 25 to day 70. The largest drop in CAP magnitudes occurred between day 50 and day 70, with responses of 70-day-old flies even falling below those of 1-day-old flies. Transducer mechanics, in contrast, remained more intact throughout. However, at day 70 the four principal parameters of transducer function, i.e. the number of sensitive transducer channels N_s), the number of insensitive transducer channels (N_i), the sensitive single channel gating force (z_s) and the insensitive single channel gating force (z_i) were all significantly different from their values at day 1, in both males and females (Mann-Whitney U test, $p<0.01$ for all). Interestingly, no such change was observed for the stiffness of the antennal joint (K_{steady}), which is a transducer-independent measure of antennal mechanics. Next to these properties shared between males and females, our analyses also revealed some sexually dimorphic phenomena: K_{GS} was significantly different only in males (Mann-Whitney U test, $p<0.01$). Whereas in females N_s, N_i, z_s and z_i, remain at constant values until the age of 50 days, the respective values of male flies change monotonously throughout the life course, with continually falling numbers of transducer channels being compensated by increasing single channel gating forces (thereby homeostatically balancing the male antenna's nonlinear stiffness). [all error bars are SEM; sample sizes males: n(day 1)=8, n(day 25)=10, n(day 50)=10), n(day 70)=8; sample sizes females: n(day 1)=11, n(day 25)=10, n(day 50)=10), n(day 70)=7]

Figure 2. Gene-Ontology and Bioinformatics of the *Drosophila* age-variable JO transcriptome

(a) Gene Ontology (GO) based summary of age-variable genes in JO as derived from RNAseq data taken across different age points (days 1, 5, 10, 25 and 50). Down-regulated (blue) and up-regulated (red) genes from multiple pairwise comparisons between all age points are shown on the left and right side of the graph, respectively. The bubble diameter is proportional to the gene number (the larger the diameter the more genes were down -or up-regulated. The y-axis shows numbers of the genes and the x-axis the Log_2Fold-Change (Log_2FC) of gene expression. GO terms correspond to the up-regulated (right) or down-regulated (left) genes, a selection of which is shown in the respective neighbouring boxes; enrichment scores are shown in brackets. Selection of the most age variable genes are shown in individual boxes corresponding to each GO term next to it. Individual bubbles denote the number of genes (y-position of bubble centre) and their corresponding range of Log_2FC values; negative ranges like '-1<x<-0.59' mean that genes were downregulated between 2^1 and $2^{0.59}$ times, whereas positive ranges like '1<x<0.59' denote an upregulation between 2^1 and $2^{0.59}$ times. (b) Prediction of upstream transcriptional master regulators for age-variable JO target genes (based on motif-binding analysis in the *i*Regulon software package). Identified master regulators *wor, amos, Optix* and *onecut* are shown in yellow with arrows leading to their predicted targets. Targets are grouped, up and down-regulated genes shown in blue and red, respectively. Mechanosensory ion channels, previously linked to fly hearing, are shown in green: *iav* and *nompC* are predicted to be downstream of *onecut*, *amos* and *Optix*, whereas *nan* is predicted to be downstream of *wor*, *Optix* and *onecut*.

Figure 3. Expression validation of homeostatic master regulators in JO

All four predicted regulators (Wor, Amos, Optix and Onecut) are expressed in JO (expression analysis was done at the age of day 10 for all genotypes). Expression of Wor was detected by expressing EGFP under the control of a *wor*-Gal4 driver; expression of Amos, Optix and Onecut was detected by using GFP-tagged flyFos gene expression constructs [78]. Co-labelling with antibodies against two pan-neuronal markers (the nuclear marker Elav, red; and the membrane marker HRP, blue) confirmed neuronal expression for all four regulators. Arrowheads indicate examples of clear co-localization between the three signals.

Figure 4. Functional validation of homeostatic master regulators

(a) Average vibration velocities of female unstimulated sound receivers ('free fluctuations') after adult-specific, RNAi-mediated knockdown (KD; red solid lines) for all four master regulators alongside their respective controls (grey dashed lines). KDs of *amos* and *onecut* show a loss of sound receiver function, as evident from (i) reduced energy content ('power gain'), (ii) reduced frequency selectivities, and - in the case of *onecut* - also (iv) best frequency shifts towards higher values. KDs of *wor* and *Optix*, in contrast, show enhanced sound receiver function, as evident from (i) increased energy content and (ii) increased frequency selectivity (*wor*) or best frequency shifts to lower values (*Optix*). [Supplementary Table 6 for numerical details and statistics]. All flies were assessed 15 days after eclosion.

(b) Line plot summaries comparing the KD sound receiver phenotypes [as from (a)] to the sound receiver phenotypes occurring naturally during ageing (reference for comparison: Canton-S day 1 to day 70). Arrows indicate significant changes in parameters. Black arrows indicate that KD phenotypes (relative to their corresponding controls) phenocopy the age-related hearing loss (ARHL) phenotypes seen in wildtype flies. White arrows indicate a reversal of the specific ARHL phenotype.

(c) Gating compliances (average fits, top) and CAP responses (medians plus standard errors, bottom) to force step actuation across adult-specific KDs of four master regulators (red) and their corresponding controls (grey). CAP responses are plotted against both stimulus force and antennal displacements. KD of *onecut* leads to a dramatic loss of auditory transducer function, as evident from the near complete loss of the gating compliance for the most

sensitive transducers and the loss of nerve responses to small stimulus forces/displacements. KDs of *wor*, *amos* and *Optix* have subtler effects on transducer mechanics but all reduce nerve responses to larger stimulus forces/displacements.
(d) Line plot summaries of transducer mechanics [from (C)] in four regulator KDs (red) relative to controls (green). Dashed lines indicate respective control values. Significant changes are asterisked (*).
(e) Sound-induced behavioural responses in males after *wor*, *amos*, *Optix* and *onecut* KD (red) compared to control flies (grey). *wor* KD mutants show hypersensitivity to sound and show significant reduction of locomotor activity to sound compared to the baseline (n=14,p= 0.029, Mann-Whitney Rank Sum Test), *amos* KD mutants do not respond to sound (n=12, p= 0.503, t-test), *Optix* KD mutants show hypersensitivity to sound and show significant reduction of locomotor activity to sound compared to the baseline (n=17,p= 0.001, Mann-Whitney Rank Sum Test), *onecut* KD mutants do not respond to sound (n=10, p=0.277, t-test), while their respective controls show an increase in locomotor activities in response to sound (n=36, p= <0.001, Mann-Whitney Rank Sum Test).

Figure 5. Key molecular targets validation and gene therapeutic approach to ARHL
(a) Gene expression changes after regulator KDs as quantified by RT-qPCR. *wor* and *amos* KDs show significant reduction of the dynein motor Dhc98D, while KD of *Optix* leads to overexpression of NompC; *onecut* KD reduces expression of both *nan* and *iav*. (*n* indicates the biological replicates, error bars show standard deviations, *p> 0.05, **p>0.01).
(b) Vibration velocity of the sound-receiver and the sharpness of the tuning Q are significantly reduced in *Dhc98D* knockdown flies (shown in red) compared to the controls (shown in dotted grey). See also Supplementary Table 6.

(c) Power Spectral Densities of unstimulated antennal sound receivers betray accelerated age-related hearing loss (aARHL) in flies kept at 30 °C (left), with a near complete loss of receiver activity already at ~day 25 (light blue area: 1 day old flies; dark blue area: 25 day old flies). A 30-day-long *amos* (middle) overexpression (OE) or *wor* (right) knockdown (at 30 °C) protects receivers from the age-related loss of activity (dark blue: KD or OE, respectively; light blue: controls). Box plots show energy contents (power gains) for each transgenic intervention (dark blue) relative to controls (light blue).

Figure 6. Comparison of lifespan and auditory healthspan
The flies' auditory health span (here depicted as median auditory gain in % of its maximum value) and survival rates (three independent cohorts shown) are closely aligned. Both show sharp drops from ~50 days on (stocks kept at 25°C and 60% relative humidity).

Table 1. Previously identified JO genes with age-variable expression

36.7 % (108 out of 294) of all previously reported JO genes show age variable expression patterns. Genes highlighted in **bold** are changing their expression mainly in males. Please note that many genes previously identified (Senthilan et al. 2012)[28], such as rhodopsins, the mechanosensitive ion channel Nan, the ATP pumps nervanas, innexins, tilB etc., show high variability in JO across ages. 'Avg exp' stands for 'Average expression'.

Table 2. Mouse genes linked to deafness, which are conserved - and expressed - in the *Drosophila* JO.

68% (105 out of 154) of all reported mammalian/human hearing loss genes are conserved in *Drosophila* and expressed in JO; 31% (33/105) are changing with age (shown in **bold** type). Novel candidate genes for mammalian/human hearing loss, recently identified are underlined. References (Ref.): (1) [Bowl R. et al. 2017][12] ; (2) [Ingham N. et al. 2019][13]; (3) [Potter P. et al. 2016][14]; (4) [Wells H. et al. 2019][15]. 'Avg exp' stands for 'Average expression'.

REFERENCES

1 WHO. *WHO Deafness and Hearing*, <http://www.who.int/news-room/fact-sheets/detail/deafness-and-hearing-loss> (2018).

2 Gates, G. A. & Mills, J. H. Presbycusis. *Lancet* **366**, 1111-1120, doi:Doi 10.1016/S0140-6736(05)67423-5 (2005).

3 Christensen, K., Frederiksen, H. & Hoffman, H. J. Genetic and environmental influences on self-reported reduced hearing in the old and oldest old. *J Am Geriatr Soc* **49**, 1512-1517, doi:DOI 10.1046/j.1532-5415.2001.4911245.x (2001).

4 Yamasoba, T. *et al.* Current concepts in age-related hearing loss: Epidemiology and mechanistic pathways. *Hearing Research* **303**, 30-38, doi:10.1016/j.heares.2013.01.021 (2013).

5 Someya, S. *et al.* Age-related hearing loss in C57BL/6J mice is mediated by Bak-dependent mitochondrial apoptosis. *Proceedings of the National Academy of Sciences of the United States of America* **106**, 19432-19437, doi:10.1073/pnas.0908786106 (2009).

6 Johnson, K. R., Erway, L. C., Cook, S. A., Willott, J. F. & Zheng, Q. Y. A major gene affecting age-related hearing loss in C57BL/6J mice. *Hearing Research* **114**, 83-92, doi:https://doi.org/10.1016/S0378-5955(97)00155-X (1997).

7 Johnson, K. R., Zheng, Q. Y. & Erway, L. C. A Major Gene Affecting Age-Related Hearing Loss Is Common to at Least Ten Inbred Strains of Mice. *Genomics* **70**, 171-180, doi:https://doi.org/10.1006/geno.2000.6377 (2000).

8 Johnson, K. R. *et al.* Separate and combined effects of Sod1 and Cdh23 mutations on age-related hearing loss and cochlear pathology in C57BL/6J mice. *Hearing research* **268**, 85-92, doi:10.1016/j.heares.2010.05.002 (2010).

9 Avraham, K. B. *et al.* The mouse Snell's waltzer deafness gene encodes an unconventional myosin required for structural integrity of inner ear hair cells. *Nature genetics* **11**, 369-375, doi:10.1038/ng1295-369 (1995).

10 Gibson, F. *et al.* A type VII myosin encoded by the mouse deafness gene shaker-1. *Nature* **374**, 62, doi:10.1038/374062a0 (1995).

11 Someya, S. *et al.* Sirt3 Mediates Reduction of Oxidative Damage and Prevention of Age-Related Hearing Loss under Caloric Restriction. *Cell* **143**, 802-812, doi:https://doi.org/10.1016/j.cell.2010.10.002 (2010).

12 Bowl, M. R. *et al.* A large scale hearing loss screen reveals an extensive unexplored genetic landscape for auditory dysfunction. *Nature Communications* **8**, 886, doi:10.1038/s41467-017-00595-4 (2017).

13 Ingham, N. J. *et al.* Mouse screen reveals multiple new genes underlying mouse and human hearing loss. *PLOS Biology* **17**, e3000194, doi:10.1371/journal.pbio.3000194 (2019).

14 Potter, P. K. *et al.* Novel gene function revealed by mouse mutagenesis screens for models of age-related disease. *Nature Communications* **7**, 13, doi:10.1038/ncomms12444 (2016).

15 Wells, H. R. R. *et al.* GWAS Identifies 44 Independent Associated Genomic Loci for Self-Reported Adult Hearing Difficulty in UK Biobank. *Am J Hum Genet* **105**, 788-802, doi:10.1016/j.ajhg.2019.09.008 (2019).

16 Albert, J. T., Nadrowski, B. & Göpfert, M. C. Mechanical signatures of transducer gating in the *Drosophila* ear. *Curr Biol* **17**, 1000-1006, doi:10.1016/j.cub.2007.05.004 (2007).

17 Nadrowski, B., Albert, J. T. & Gopfert, M. C. Transducer-based force generation explains active process in Drosophila hearing. *Current Biology* **18**, 1365-1372, doi:10.1016/j.cub.2008.07.095 (2008).

18 Göpfert, M. C., Humphris, A. D., Albert, J. T., Robert, D. & Hendrich, O. Power gain exhibited by motile mechanosensory neurons in Drosophila ears. *Proceedings of the National Academy of Sciences of the United States of America* **102**, 325-330, doi:10.1073/pnas.0405741102 (2005).

19 Kamikouchi, A. *et al.* The neural basis of Drosophila gravity-sensing and hearing. *Nature* **458**, 165, doi:10.1038/nature07810 (2009).
20 Jarman, A. P., Grau, Y., Jan, L. Y. & Jan, Y. N. atonal is a proneural gene that directs chordotonal organ formation in the Drosophila peripheral nervous system. *Cell* **73**, 1307-1321 (1993).
21 Bermingham, N. A. *et al.* Math1: an essential gene for the generation of inner ear hair cells. *Science* **284**, 1837-1841 (1999).
22 Wang, V. Y., Hassan, B. A., Bellen, H. J. & Zoghbi, H. Y. *Drosophila* atonal fully rescues the phenotype of Math1 null mice: New functions evolve in new cellular contexts. *Current Biology* **12**, 1611-1616, doi:10.1016/S0960-9822(02)01144-2 (2002).
23 Weinberger, S. *et al.* Evolutionary changes in transcription factor coding sequence quantitatively alter sensory organ development and function. *eLife* **6**, e26402, doi:10.7554/eLife.26402 (2017).
24 Li, T. C., Bellen, H. J. & Groves, A. K. Using Drosophila to study mechanisms of hereditary hearing loss. *Dis. Model. Mech.* **11**, 16, doi:10.1242/dmm.031492 (2018).
25 Kavlie, R. G. *et al.* Prestin is an anion transporter dispensable for mechanical feedback amplification in Drosophila hearing. *J. Comp. Physiol. A -Neuroethol. Sens. Neural Behav. Physiol.* **201**, 51-60, doi:10.1007/s00359-014-0960-9 (2015).
26 Kamikouchi, A., Albert, J. T. & Gopfert, M. C. Mechanical feedback amplification in Drosophila hearing is independent of synaptic transmission. *European Journal of Neuroscience* **31**, 697-703, doi:10.1111/j.1460-9568.2010.07099.x (2010).
27 Karak, S. *et al.* Diverse Roles of Axonemal Dyneins in Drosophila Auditory Neuron Function and Mechanical Amplification in Hearing. *Scientific Reports* **5**, doi:10.1038/srep17085 (2015).
28 Senthilan, P. R. *et al.* Drosophila auditory organ genes and genetic hearing defects. *Cell* **150**, 1042-1054, doi:10.1016/j.cell.2012.06.043 (2012).
29 Kavlie, R. G. & Albert, J. T. Chordotonal organs. *Current Biology* **23**, R334-R335 (2013).
30 Kamikouchi, A., Shimada, T. & Ito, K. Comprehensive classification of the auditory sensory projections in the brain of the fruit fly *Drosophila* melanogaster. *J Comp Neurol* **499**, 317-356, doi:10.1002/cne.21075 (2006).
31 von Schilcher, F. The role of auditory stimuli in the courtship of *Drosophila melanogaster*. *Animal Behaviour* **24**, 18-26 (1976).
32 Ruhmann, H., Koppik, M., Wolfner, M. F. & Fricke, C. The impact of ageing on male reproductive success in Drosophila melanogaster. *Experimental Gerontology* **103**, 1-10, doi:https://doi.org/10.1016/j.exger.2017.12.013 (2018).
33 Prathibha, M., Krishna, M. S. & Jayaramu, S. C. Male age influence on male reproductive success in Drosophila ananassae (Diptera: Drosophilidae). *Ital. J. Zoolog.* **78**, 168-173, doi:10.1080/11250003.2011.564214 (2011).
34 Albert, Joerg T. & Kozlov, Andrei S. Comparative Aspects of Hearing in Vertebrates and Insects with Antennal Ears. *Current Biology* **26**, R1050-R1061, doi:10.1016/j.cub.2016.09.017 (2016).
35 Markin, V. S. & Hudspeth, A. J. Gating-Spring Models of Mechanoelectrical Transduction by Hair Cells of the Internal Ear. *Annual Review of Biophysics and Biomolecular Structure* **24**, 59-83, doi:10.1146/annurev.bb.24.060195.000423 (1995).
36 Albert, J. T., Nadrowski, B. & Göpfert, M. C. *Drosophila* mechanotransduction - Linking proteins and functions. *Fly* **1**, 238-241 (2007).
37 Eden, E., Lipson, D., Yogev, S. & Yakhini, Z. Discovering motifs in ranked lists of DNA sequences. *Plos Computational Biology* **3**, 508-522, doi:10.1371/journal.pcbi.0030039 (2007).
38 Eden, E., Navon, R., Steinfeld, I., Lipson, D. & Yakhini, Z. GOrilla: a tool for discovery and visualization of enriched GO terms in ranked gene lists. *Bmc Bioinformatics* **10**, doi:10.1186/1471-2105-10-48 (2009).

39 Roy, M., Sivan-Loukianova, E. & Eberl, D. F. Cell-type–specific roles of Na+/K+ ATPase subunits in Drosophila auditory mechanosensation. *Proceedings of the National Academy of Sciences* **110**, 181-186, doi:10.1073/pnas.1208866110 (2013).

40 Christie, K. W. *et al.* Physiological, anatomical, and behavioral changes after acoustic trauma in Drosophila melanogaster. *Proceedings of the National Academy of Sciences of the United States of America* **110**, 15449-15454, doi:DOI 10.1073/pnas.1307294110 (2013).

41 Janky, R. s. *et al.* iRegulon: From a Gene List to a Gene Regulatory Network Using Large Motif and Track Collections. *PLOS Computational Biology* **10**, e1003731, doi:10.1371/journal.pcbi.1003731 (2014).

42 Dubruille, R. *et al.* Drosophila regulatory factor X is necessary for ciliated sensory neuron differentiation. *Development* **129**, 5487-5498, doi:10.1242/dev.00148 (2002).

43 Ebacher, D. J. S., Todi, S. V., Eberl, D. F. & Falk, G. E. B. cut mutant Drosophila auditory organs differentiate abnormally and degenerate. *Fly* **1**, 86-94, doi:10.4161/fly.4242 (2007).

44 Kim, J. *et al.* A TRPV family ion channel required for hearing in Drosophila. *Nature* **424**, 81-84, doi:10.1038/nature01733 (2003).

45 Gong, Z. *et al.* Two Interdependent TRPV Channel Subunits, Inactive and Nanchung, Mediate Hearing in <em>Drosophila</em&gt. *The Journal of Neuroscience* **24**, 9059 (2004).

46 Effertz, T., Wiek, R. & Gopfert, M. C. NompC TRP Channel Is Essential for Drosophila Sound Receptor Function. *Current Biology* **21**, 592-597, doi:10.1016/j.cub.2011.02.048 (2011).

47 Kirkwood, T. B. L. Evolution of Aging. *Nature* **270**, 301-304, doi:DOI 10.1038/270301a0 (1977).

48 Gems, D. & Partridge, L. in *Annual Review of Physiology, Vol 75* Vol. 75 *Annual Review of Physiology* (ed D. Julius) 621-644 (Annual Reviews, 2013).

49 Nguyen, D. N. T., Rohrbaugh, M. & Lai, Z.-C. The Drosophila homolog of Onecut homeodomain proteins is a neural-specific transcriptional activator with a potential role in regulating neural differentiation. *Mechanisms of Development* **97**, 57-72, doi:https://doi.org/10.1016/S0925-4773(00)00431-7 (2000).

50 Wu, F., Sapkota, D., Li, R. & Mu, X. Onecut 1 and Onecut 2 are potential regulators of mouse retinal development. *The Journal of Comparative Neurology* **520**, 952-969, doi:10.1002/cne.22741 (2012).

51 Nesterov, A. *et al.* TRP Channels in Insect Stretch Receptors as Insecticide Targets. *Neuron* **86**, 665-671, doi:http://dx.doi.org/10.1016/j.neuron.2015.04.001 (2015).

52 Lehnert, B. P., Baker, A. E., Gaudry, Q., Chiang, A.-S. & Wilson, R. I. Distinct Roles of TRP Channels in Auditory Transduction and Amplification in Drosophila. *Neuron* **77**, 115-128, doi:10.1016/j.neuron.2012.11.030 (2013).

53 Effertz, T., Nadrowski, B., Piepenbrock, D., Albert, J. T. & Göpfert, M. C. Direct gating and mechanical integrity of Drosophila auditory transducers require TRPN1. *Nature Neuroscience* **15**, 1198-1200, doi:http://dx.doi.org/10.1038/nn.3175 (2012).

54 Gopfert, M. C., Albert, J. T., Nadrowski, B. & Kamikouchi, A. Specification of auditory sensitivity by Drosophila TRP channels. *Nature Neuroscience* **9**, 999-1000, doi:10.1038/nn1735 (2006).

55 Yan, Z. *et al.* Drosophila NOMPC is a mechanotransduction channel subunit for gentle-touch sensation. *Nature* **493**, 221-225, doi:http://www.nature.com/nature/journal/v493/n7431/abs/nature11685.html#supplementary-information (2013).

56 Zhang, W. *et al.* Ankyrin Repeats Convey Force to Gate the NOMPC Mechanotransduction Channel. *Cell* **162**, 1391-1403, doi:10.1016/j.cell.2015.08.024 (2015).

57 Lai, S.-L., Miller, Michael R., Robinson, Kristin J. & Doe, Chris Q. The Snail Family Member Worniu Is Continuously Required in Neuroblasts to Prevent Elav-Induced Premature Differentiation. *Developmental Cell* **23**, 849-857, doi:10.1016/j.devcel.2012.09.007.

58 Seimiya, M. & Gehring, W. J. The Drosophila homeobox gene optix is capable of inducing ectopic eyes by an eyeless-independent mechanism. *Development* **127**, 1879 (2000).

59 Jarman, A. P., Sun, Y., Jan, L. Y. & Jan, Y. N. Role of the proneural gene, atonal, in formation of Drosophila chordotonal organs and photoreceptors. *Development* **121**, 2019-2030 (1995).

60 Jarman, A. P., Grell, E. H., Ackerman, L., Jan, L. Y. & Jan, Y. N. Atonal is the proneural gene for Drosophila photoreceptors. *Nature* **369**, 398-400, doi:10.1038/369398a0 (1994).

61 Gupta, B. P. & Rodrigues, V. Atonal is a proneural gene for a subset of olfactory sense organs in Drosophila. *Genes to cells : devoted to molecular & cellular mechanisms* **2**, 225-233 (1997).

62 Goulding, S. E., zur Lage, P. & Jarman, A. P. amos, a proneural gene for Drosophila olfactory sense organs that is regulated by lozenge. *Neuron* **25**, 69-78 (2000).

63 Huang, M. L., Hsu, C. H. & Chien, C. T. The proneural gene amos promotes multiple dendritic neuron formation in the Drosophila peripheral nervous system. *Neuron* **25**, 57-67 (2000).

64 Maung, S. M. & Jarman, A. P. Functional distinctness of closely related transcription factors: a comparison of the Atonal and Amos proneural factors. *Mech Dev* **124**, 647-656, doi:10.1016/j.mod.2007.07.006 (2007).

65 Xie, W. R. *et al.* An Atoh1-S193A Phospho-Mutant Allele Causes Hearing Deficits and Motor Impairment. *J Neurosci* **37**, 8583-8594, doi:10.1523/jneurosci.0295-17.2017 (2017).

66 Nadrowski, B. & Göpfert, M. C. Level-dependent auditory tuning: Transducer-based active processes in hearing and best-frequency shifts. *Commun Integr Biol* **2**, 7-10 (2009).

67 Zanini, D. *et al.* Proprioceptive Opsin Functions in Drosophila Larval Locomotion. *Neuron* **98**, 67-+, doi:10.1016/j.neuron.2018.02.028 (2018).

68 Ratnapriya, R. *et al.* Retinal transcriptome and eQTL analyses identify genes associated with age-related macular degeneration. *Nature genetics* **51**, 606-610, doi:10.1038/s41588-019-0351-9 (2019).

69 Schrauwen, I. *et al.* A comprehensive catalogue of the coding and non-coding transcripts of the human inner ear. *Hear Res* **333**, 266-274, doi:10.1016/j.heares.2015.08.013 (2016).

70 Kaushik, S. & Cuervo, A. M. Proteostasis and aging. *Nat. Med.* **21**, 1406-1415, doi:10.1038/nm.4001 (2015).

71 Wang, W. W. *et al.* Impaired unfolded protein response in the degeneration of cochlea cells in a mouse model of age-related hearing loss. *Experimental Gerontology* **70**, 61-70, doi:10.1016/j.exger.2015.07.003 (2015).

72 Freeman, S. *et al.* Proteostasis is essential during cochlear development for neuron survival and hair cell polarity. *Embo Rep* **20**, 20, doi:10.15252/embr.201847097 (2019).

73 Hertzano, R. *et al.* Cell Type–Specific Transcriptome Analysis Reveals a Major Role for *Zeb1* and miR-200b in Mouse Inner Ear Morphogenesis. *Plos Genet* **7**, e1002309, doi:10.1371/journal.pgen.1002309 (2011).

74 Nelson, G. ONTOGENY, PHYLOGENY, PALEONTOLOGY, AND BIOGENETIC LAW. *Systematic Zoology* **27**, 324-345, doi:10.2307/2412883 (1978).

75 Richardson, M. K. A Phylotypic Stage for All Animals? *Developmental Cell* **22**, 903-904, doi:https://doi.org/10.1016/j.devcel.2012.05.001 (2012).

76 Kalinka, A. T. *et al.* Gene expression divergence recapitulates the developmental hourglass model. *Nature* **468**, 811-U102, doi:10.1038/nature09634 (2010).

77 Nitta, K. R. *et al.* Conservation of transcription factor binding specificities across 600 million years of bilateria evolution. *Elife* **4**, doi:10.7554/eLife.04837 (2015).

78 Sarov, M. *et al.* A genome-wide resource for the analysis of protein localisation in Drosophila. *eLife* **5**, e12068, doi:10.7554/eLife.12068 (2016).

79 Shimada, T., Kato, K., Kamikouchi, A. & Ito, K. Analysis of the distribution of the brain cells of the fruit fly by an automatic cell counting algorithm. *Physica A* **350**, 144-149, doi:DOI 10.1016/j.physa.2004.11.033 (2005).

80 Ling, D. & Salvaterra, P. M. Robust RT-qPCR Data Normalization: Validation and Selection of Internal Reference Genes during Post-Experimental Data Analysis. *PLOS ONE* **6**, e17762, doi:10.1371/journal.pone.0017762 (2011).
81 Inagaki, H. K., Kamikouchi, A. & Ito, K. Protocol for quantifying sound-sensing ability of Drosophila melanogaster. *Nature Protocols* **5**, 26-30, doi:10.1038/nprot.2009.206 (2010).

1155

Table 1. Previously identified JO genes with age-variable expression

36.7 % (108 out of 294) of all previously reported JO genes show age variable expression patterns. Genes highlighted in **bold** are changing their expression mainly in males. Please note that many genes previously identified (Senthilan et al. 2012)[28], such as rhodopsins, the mechanosensitive ion channel Nan, the ATP pumps nervanas, innexins, tilB etc., show high variability in JO across ages. 'Avg exp' stands for 'Average expression'.

***Drosophila* gene**	**Mouse orthologue**	**Description**	***Avg exp***
Arr2	Arrb2	Arrestin 2	10610.9
bab1	Nacc1, Nacc2	bric a brac 1	117.2
Cam	Calm3, Calm1	Calmodulin	13985.2
CG10050	Dtwd2		69.5
CG10185	Nwd2, Nwd1		10088.6
CG10257	Faim		978.5
CG10866	Tmem267		750.6
CG11041	Efcab2		836.3
CG11353	Oacyl		352.1
CG12947	Wfdc8		26.4
CG13133	Hspb2		7243.0
CG13202	Ccdc103		63.4
CG13305			90.3
CG13842	Ccdc142		850.2
CG13950	Lgals4, Lgals9		6970.4
CG14215	Ahctf1		379.9
CG14274			756.9
CG14342			512.0
CG14591	Tmem164		1102.9
CG14693	Cnbd2		574.5
CG14905	Ccdc63		306.0
CG14921	Dyx1c1		153.4
CG14947			98.1
CG15143	Maats1		411.5
CG1561			703.6
CG15878			385.3
CG15927			174.4
CG17279			2806.3
CG17352	Neto1		435.7
CG18130	Nme8		1607.7
CG18336	Fam166b		881.3
CG2681	Siah1a		88.2
CG30203	Spon1		1025.5
CG31019	Agbl4		699.3
CG32373	Scube3, Scube2		188.1
CG40485	Dhrs11		161.4
CG4660	Them6		153.7

CG5687	Slc5a6, Slc5a8, Slc5a12, Slc5a5		11118.1
CG5948	Sod3		1254.7
CG6912			411.7
CG6983	1700037H04Rik		290.1
CG7220	Ube2w		2256.9
CG8086	Odf3b		8186.2
CG8086	Odf3		8186.2
CG8369			157754.2
CG8407	Dnal4		204.2
CG8419	Trim45		155.7
CG8560	Cpb1		23.6
CG9150	Dhrs11		258.9
CG9317	Slc22a1		73.3
cpx	Cplx1, Clpx2	complexin	9601.1
Dhc36C	Dnah7b, Dnah7a, Dnah7c	Dynein heavy chain at 36C	656.9
dila	Cep131	dilatory	282.5
eys	Agrn	eyes shut	972.6
Fer1	Ptf1a	48 related 1	807.5
futsch	Map1a	futsch	4019.4
Ggamma30A	Gng13		5991.3
gol	Rnf150	goliath	381.9
hoe2	Oca2	hoepel2	358.6
inaD	Lnx2, Lnx1	inactivation no afterpotential D	401.8
Inx2		Innexin 2	1705.2
Inx5		Innexin 5	86.8
Inx7		Innexin 7	15.8
Ir100a		Ionotropic receptor 100a	55.4
Ir76a		Ionotropic receptor 76a	202.4
laza	Plpp3, Plpp1, Plpp2	lazaro	109.2
Naam		Nicotinamide amidase	11686.7
nompA		no mechanoreceptor potential A	438.9
nrv1	Atp1b1, Atp1b2	nervana 1	2020.1
nrv2	Atp1b1, Atp1b4, Atp1b2	nervana 2	14651.9
nrv3	Atp1b1	nervana 3	14857.5
Obp84a		Odorant-binding protein 84a	33.7
Osi2		Osiris 2	94.5
Pep	Ciz1	Protein on ecdysone puffs	2051.2
PIP82		PIP82	143.0
Pph13	Arx	PvuII-PstI homology 13	92.3
Prestin	Slc26a5	Prestin	655.8
pyx	Trpa1	pyrexia	342.8
retinin	Tmem38b	retinin	390.5
Rh4	Opn4	Rhodopsin 4	1817.9
Rh5	Opn4	Rhodopsin 5	441.1

Rh6	Opn4	Rhodopsin 6	1430.9
rtp	Morn4	retinophilin	634.4
Sas	Wisp2	Sialic acid phosphate synthase	203.8
se	Gsto1	sepia	118.4
stops	Asb17	slow termination of phototransduction	189.9
Tektin-C	Tekt1	Tektin C	1229.0
tilB	Lrrc6	touch insensitive larva B	110.5
tipE	Kcnmb4	temperature-induced paralytic E	1231.5
trp	Trpc5, Trpc4	transient receptor potential	1912.1
gl	**Ostm1, Lipf**	**glass**	**405.85**
qvr		**quiver**	**2018.17**
norpA	**Plcb4**	**no receptor potential A**	**2082.24**
nan	**Trpv5, Trpv6**	**nanchung**	**572.72**
dpr5	**Jaml**	**dpr5**	**379.81**
Hdc	**Hdc**	**Histidine decarboxylase**	**95.09**
MESK2	**Ndrg3**	**Misexpression suppressor of KSR 2**	**7920.87**
run	**Runx1**	**runt**	**956.47**
Ir94b		**Ionotropic receptor 94b**	**34.25**
spn-B	**Xrcc3**	**spindle B**	**246.93**
Cpr49Ag	**Gm7030**	**Cuticular protein 49Ag**	**51.42**
Eaat2	**Slc1a2**	**Excitatory amino acid transporter 2**	**1431.19**
rdgA	**Dgkz**	**retinal degeneration A**	**2225.92**
Ptpmeg	**Ptpn4**	**Ptpmeg**	**742.21**
ninaC	**Myo3a**	**neither inactivation nor afterpotential C**	**1255.66**
Bmcp	**Slc25a30**	**Bmcp**	**517.16**
CAP	**Sorbs2, Sorbs1, Sorbs3**	**CAP**	**4842.87**
oc	**Otx2, Otx1**	**ocelliless**	**437.87**

1162

1163

Table 2. Mouse genes linked to deafness, which are conserved - and expressed - in the *Drosophila* JO.

68% (105 out of 154) of all reported mammalian/human hearing loss genes are conserved in *Drosophila* and expressed in JO; 31% (33/105) are changing with age (shown in **bold** type). Novel candidate genes for mammalian/human hearing loss, recently identified are underlined. References: (1) [Bowl R. et al. 2017][12] ; (2) [Ingham N. et al. 2019][13]; (3) [Potter P. et al. 2016][14]; (4) [Wells H. et al. 2019][15]. 'Avg exp' stands for 'Average expression'.

Type of hearing loss	*Drosophila* gene	Mouse/HUMAN orthologue	Avg exp	Description	Ref.
Severe hearing loss	**mol**	**Duoxa2**	351.20	moladietz	(1)
	CG8907	**Eps8l1**	192.00		(1)
	CG32669	**Slc5a5**	30.70		
	CG5038	**Tmtc4**	119.20		(1)
	CG12104	**Tox**	227.10		(1)
	CG5921	**Ush1c**	192.90		
	Myo28B1	**Myo7a**	189.80	Myosin 28B1	
	Klc	Klc2	860.39	Kinesin light chain	(1)
	Nedd4	Nedd4l	994.11	Nedd4	(1)
	CG9947	Tmem30b	1224.37		(1)
	ck	Myo7a	358.45	crinkled	
	spin	Spns2	1121.31	spinster	
	kermit	Gipc3	220.20	kermit	
	CG5245	Zfp719	30.62		(2)
Mild hearing loss	**or**	**Ap3s1**	152.20	orange	(1)
	Mhc	**Myh1**	3541.70	Myosin heavy chain	(1)
	CG8086	**Odf3l2**	8186.20		(1)
	TRAM	**Tram2**	491.20	TRAM	(1)
	Ubc6	**Ube2b**	2237.70	Ubiquitin conjugating enzyme 6	(1)
	CG32082	Baiap2l2	1204.20		(1)
	CG5946	Cyb5r2	3204.64		(1)
	Ndae1	Slc4a10	1059.54	Na[+]-driven anion exchanger 1	(1)
	CG40045	Ube2g1	1627.07		(1)
	Ubc87F	Ube2g1	108.25	Ubiquitin conjugating enzyme 87F	(1)
	Vti1	Vti1a	135.59	VTI1 ortholog (S. cerevisiae)	(1)

	14-3-3epsilon	**Ywhae**	8321.45	14-3-3epsilon	(2)
	Klc	Klc2	860.39	Kinesin light chain	(2)
	scny	Usp42	1110.12	scrawny	(2)
	x16	Srsf7	177.56	x16 splicing factor	(2)
	CG10492	Zcchc14	482.32		(2)
	E(spl)m7-HLH	**Bhlhe40**	25.81	Enhancer of split m7, helix-loop-helix TF	(2)
	E(spl)m8-HLH	**Bhlhe40**	23.20	Enhancer of split m8, helix-loop-helix TF	(2)
	Eip63E	Cdk14	1185.21	Ecdysone-induced protein 63E	(2)
	Poxm	**Pax9**	58.68	Pox meso TF	(2)
	MCPH1	Mcph1	487.34	Microcephalin	(2)
	lbk	**Lrig1**	1089.47	lambik	(2)
	gish	Csnk1g3	1763.59	gilgamesh	(2)
	CG9328	Fam107b	905.33		(2)
	MBD-R2	**Phf20**	322.21	MBD-R2, Zinc finger C2H2 TF	(2)
	upSET	Setd5	1537.11	transcriptional regulator	(2)
	pigs	Gas2l2	1788.66	pickled eggs	(2)
	HERC2	Herc1	361.78	HECT and RLD domain containing protein 2	(2)
High frequency	**Acsl**	**Acsl4**	3654.70	Acyl-CoA synthetase long-chain	(1)
hearing loss	Nak	Aak1	2333.08	Numb-associated kinase	(1)
	Bsg	Emb	6407.84	Basigin, IgG family glycoprotein	(1)
	Bsg25D	Nin	905.62	Blastoderm-specific gene 25D	(1)
	alph	Ppm1a	1077.38	alphabet, Ser/Thr phosphatase	(1)
	adp	Wdtc1	359.91	adipose, lipid metabolism gene	(1)
	Girdin	Ccdc88c	562.48	Girdin	(1)
	caz	Ewsr1	389.75	cabeza, chromatin binding protein	(1)
	Pex3	Pex3	767.87	Peroxin 3, peroxisomal membrane protein	(2)
	Wbp2	Wbp2	3401.51	WW domain binding protein 2	(2)
	CenG1A	Agap1	610.62	Centaurin gamma 1A, GTPase	(2)
	CG17928	Fads3	1637.19		(2)

	Cyt-b5-r	Fads3	1636.01	Cytochrome b5-related	(2)
	CG4911	Fbxo33	1078.38		(2)
	fs(1)h	Brd2	4452.95	female sterile (1) homeotic	(2)
Low frequency	**srp**	**Gata2**	250.10	serpent, GATA TF	
hearing loss	grn	Gata2	210.30	grain, GATA TF	
	Tre1	**Gpr50**	402.10	Trapped in endoderm 1, G protein-coupled receptor of the rhodopsin class	(1)
	PMCA	Atp2b1	2544.12	plasma membrane calcium ATPase	(1)
	KLHL18	Klhl18	419.41	Kelch like family member 18	(1)
	MED28	Med28	189.86	Mediator complex subunit 28	(1)
	NFAT	Nfatc3	1656.90	NFAT homolog	(1)
	CG10492	Zcchc14	482.32		(1)
Age-related	Patronin	Camsap3	668.15	Patronin, microtubule minus-end binding protein	(2)
hearing loss	Ndae1	Slc4a10	1059.54	Na[+]-driven anion exchanger 1	(3)
	nSyb	**Vamp2**	3748.86	neuronal Synaptobrevin	(3)
	CG5270	**Zfyve26**	281.68		(3)
	CG33158	Efl1	181.77		(3)
	TrpRS-m	Wars2	362.60	mitochondrial Tryptophanyl-tRNA synthetase	(3)
	ECSIT	Ecsit	143.05	ECSIT	(3)
	Jhe	Ces2f	549.53	Juvenile hormone esterase	(3)
	l(1)G0156	**Idh3a**	2956.36	lethal (1) G0156	(3)
	LanA	**Lama5**	1584.27	LamininA	(3)
GWAS study	eya	EYA4	95.30	eyes absent TF	(4)
	ds	**CDH23**	341.19	dachsous cadherin	(4)
	CadN2	**CDH23**	479.50	Cadherin-N2	(4)
	Cad88C	**CDH23**	789.23	Cadherin 88C	(4)
	CG1812	KLHDC7B	241.13		(4)
	osp	TRIOBP	1233.49	outspread	(4)
	CG10188	ARHGEF28	271.81		(4)
	CG6833	**ISG20**	180.20		(4)
	mGluR	GRM7	231.47	metabotropic Glutamate Receptor	(4)

	Ndg	NID2	213.82	Nidogen/entactin	(4)
	CG1103	**CLRN2**	247.68		(4)
	CG9776	ZNF318	867.16		(4)
	CG32082	BAIAP2L2	1204.20		(4)
	CG9981	ATP11B	24.59		(4)
	CG4301	ATP11B	484.18		(4)
	CG42321	ATP11B	1822.67		(4)
	CG5004	PHLDB1	339.28		(4)
	ktub	TUB	257.23	king tubby, ciliary motility protein	(4)
	AGO1	AGO2	3200.86	Argonaute-1 miRISC complex protein	(4)
	AGO2	AGO2	1251.61	Argonaute-2 RISC complex protein	(4)
	luna	KLF7	835.24	Zinc finger C2H2 transcription factor	(4)
	Synj	SYNJ2	634.20	Synaptojanin	(4)
	pico	GRB10	1137.50		(4)
	CtBP	CTBP2	2796.86	C-terminal Binding Protein	(4)
	Mctp	MCTP1	1341.93	Multiple C2 domain and transmembrane region protein	(4)
	Sec15	EXOC6	383.36	Secretory 15	(4)
	CG34422	ARID5B	186.44		(4)
	AdenoK	**ADK**	1024.37	Adenosine Kinase	(4)
	CG3809	**ADK**	8.65		(4)
	Ady43A	**ADK**	1045.60	Adenosine Kinase 43A	(4)
	dop	MAST2	916.03	drop out	(4)
	lap	SNAP91	1583.20	like-AP180	(4)
	Erk7	MAPK6	116.92	Extracellularly regulated kinase 7	(4)
	p38c	MAPK6	34.57	p38 MAP kinase	(4)
	caup	IRX2	59.69	caupolican TF	(4)
	CG7461	**ACADVL**	1638.45		(4)
	CG32105	**LMX1A**	71.81		(4)
	CG4328	LMX1A	24.64		(4)
	Lis-1	PAFAH1B1	2805.58	Lissencephaly-1, regulator of dynein motor complex	(4)

	shrb	**CHMP4C**	1275.18	shrub, ESCRT-III complex protein	(4)
	Sox14	**SOX4**	900.65	Sox box protein 14 TF	(4)
	Sox21a	**SOX4**	74.69	Sox box protein 21a TF	(4)
	Sox21b	SOX4	170.22	Sox box protein 21b TF	(4)
	D	SOX4	598.22	Dichaete TF	(4)
	SoxN	SOX4	521.37	SoxNeuro TF	(4)
	Gfrl	GFRA2	1461.90	Glial cell line-derived neurotrophic family receptor-like	(4)
	NnaD	**AGBL2**	826.98	Nna1 carboxypeptidase	(4)
	CG6867	OLFM4	545.37		(4)
	Akt1	AKT3	1176.36	core kinase of Insulin pathway	(4)
	beta-Spec	SPTBN1	2861.76	beta Spectrin	(4)

1171

1172

Figure 1.

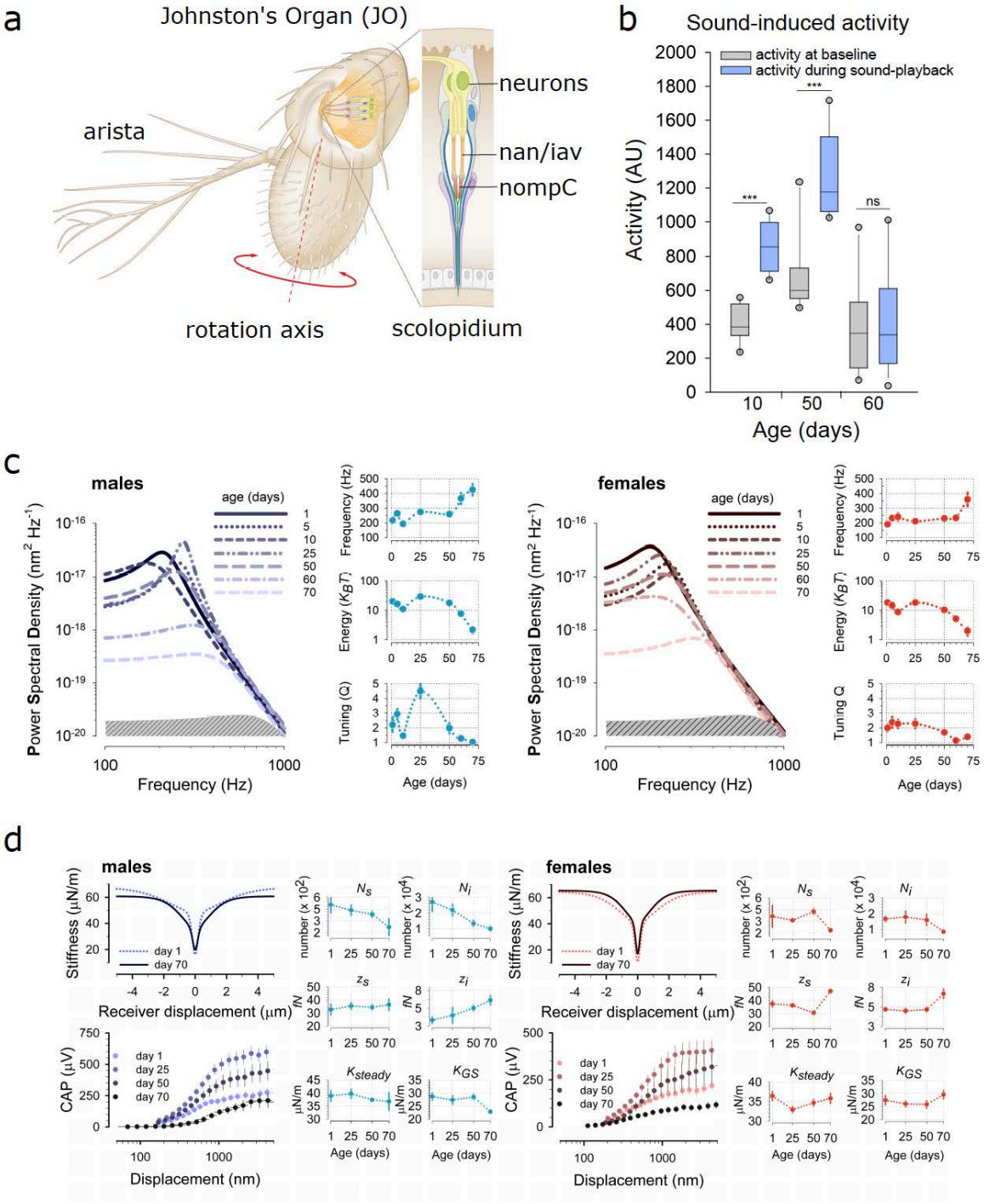

1173

1174

Figure 2.

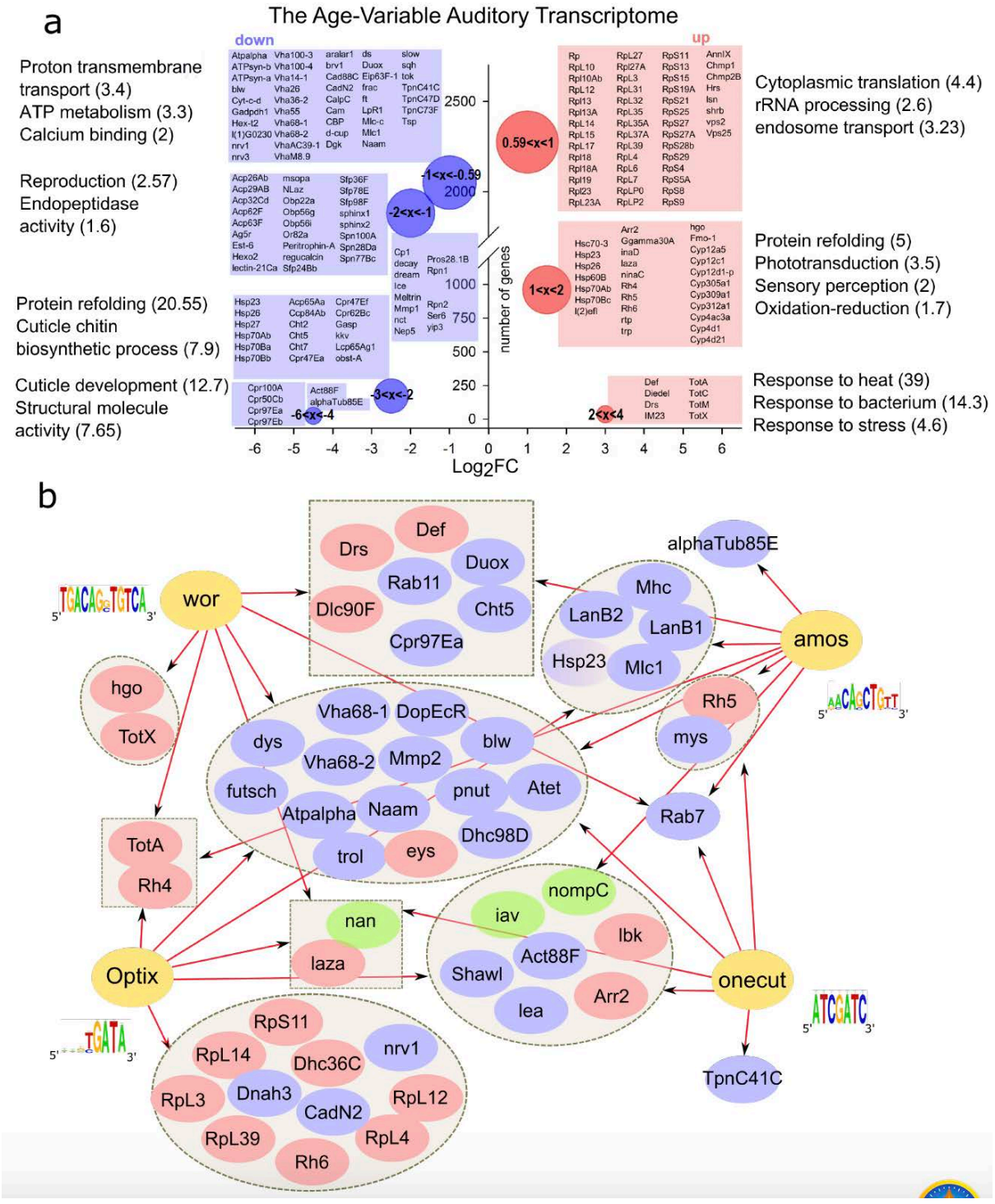
a
The Age-Variable Auditory Transcriptome
down
up
Proton transmembrane transport (3.4)
ATP metabolism (3.3)
Calcium binding (2)
Reproduction (2.57)
Endopeptidase activity (1.6)
Protein refolding (20.55)
Cuticle chitin biosynthetic process (7.9)
Cuticle development (12.7)
Structural molecule activity (7.65)
Cytoplasmic translation (4.4)
rRNA processing (2.6)
endosome transport (3.23)
Protein refolding (5)
Phototransduction (3.5)
Sensory perception (2)
Oxidation-reduction (1.7)
Response to heat (39)
Response to bacterium (14.3)
Response to stress (4.6)
number of genes
Log2FC
b
wor
amos
Optix
onecut
Rab7
TpnC41C
alphaTub85E
Def
Drs
Duox
Rab11
Dlc90F
Cht5
Cpr97Ea
Mhc
LanB2
LanB1
Hsp23
Mlc1
hgo
TotX
Vha68-1
DopEcR
dys
Vha68-2
Mmp2
blw
futsch
pnut
Atet
Atpalpha
Naam
Dhc98D
trol
eys
Rh5
mys
TotA
Rh4
nan
laza
nompC
iav
lbk
Act88F
Shawl
Arr2
lea
RpS11
RpL14
nrv1
Dhc36C
RpL3
Dnah3
CadN2
RpL12
RpL39
RpL4
Rh6

Figure 3.

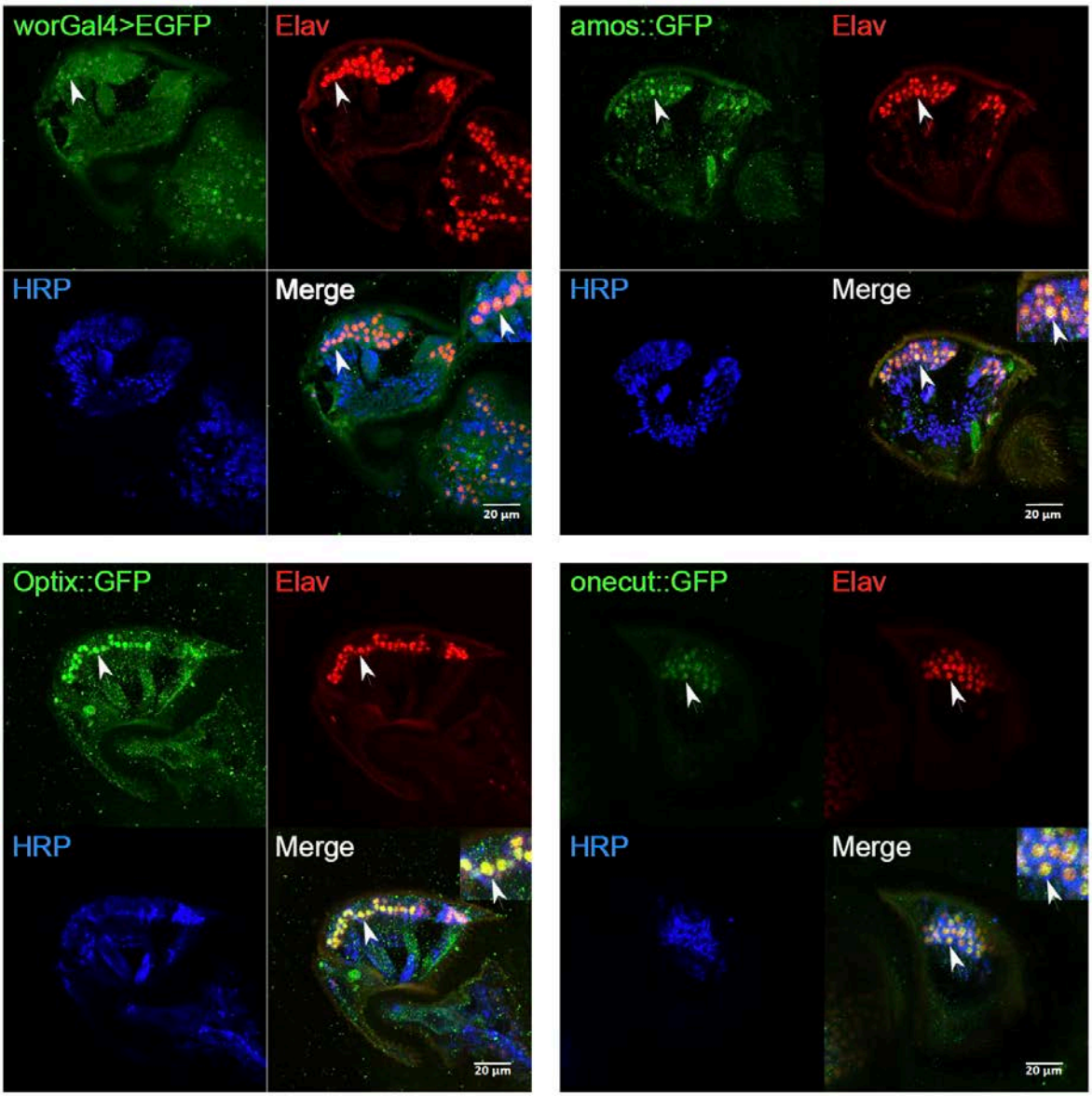

1178

1179

Figure 4.

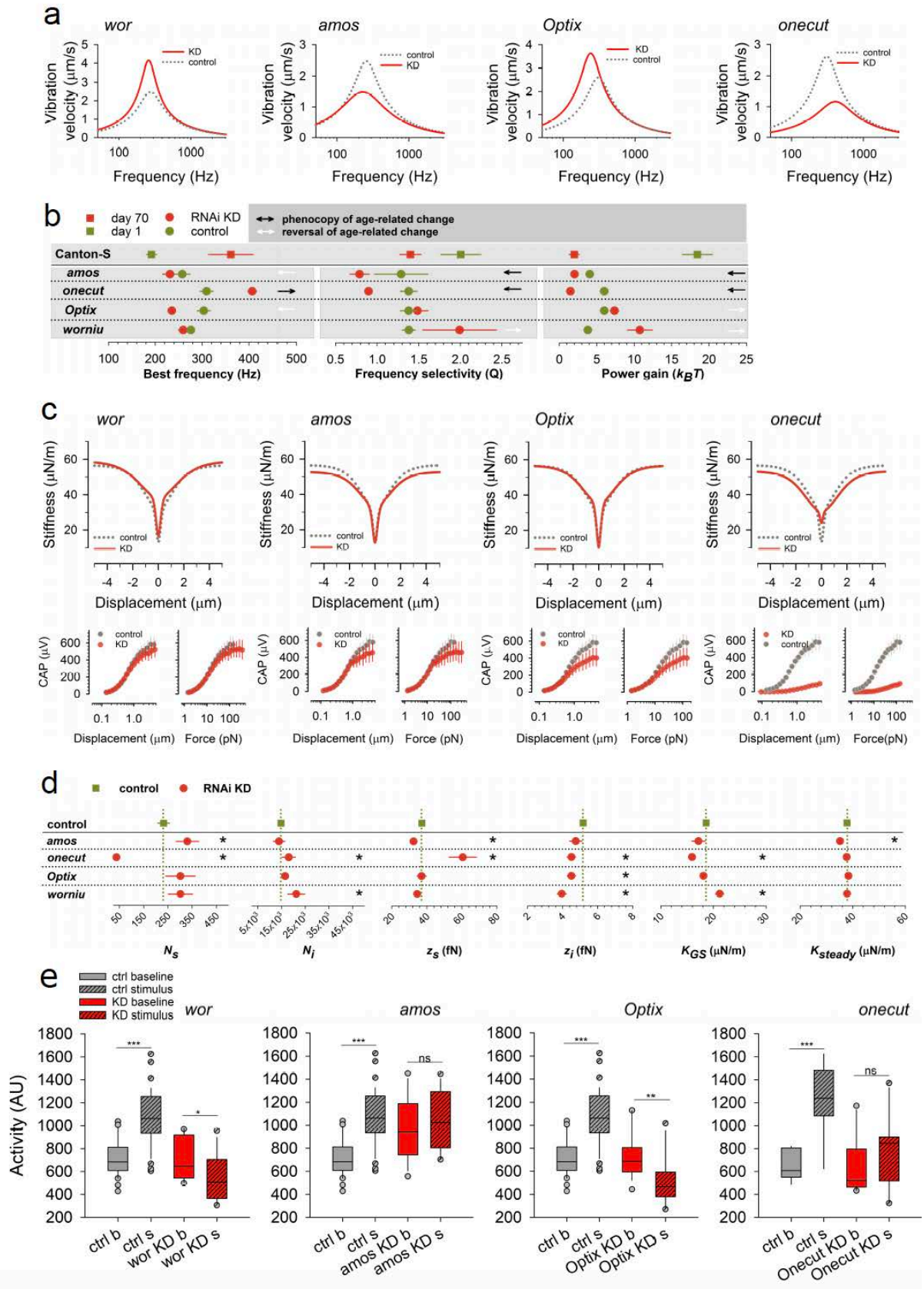
a
wor
amos
Optix
onecut
Vibration velocity (μm/s)
Frequency (Hz)
KD
control
b
day 70
day 1
RNAi KD
control
phenocopy of age-related change
reversal of age-related change
Canton-S
amos
onecut
Optix
worniu
Best frequency (Hz)
Frequency selectivity (Q)
Power gain (kBT)
c
Stiffness (μN/m)
Displacement (μm)
CAP (μV)
Force (pN)
d
control
RNAi KD
Ns
Ni
zs (fN)
zi (fN)
KGS (μN/m)
Ksteady (μN/m)
e
ctrl baseline
ctrl stimulus
KD baseline
KD stimulus
Activity (AU)
ctrl b
ctrl s
wor KD b
wor KD s
amos KD b
amos KD s
Optix KD b
Optix KD s
Onecut KD b
Onecut KD s
ns

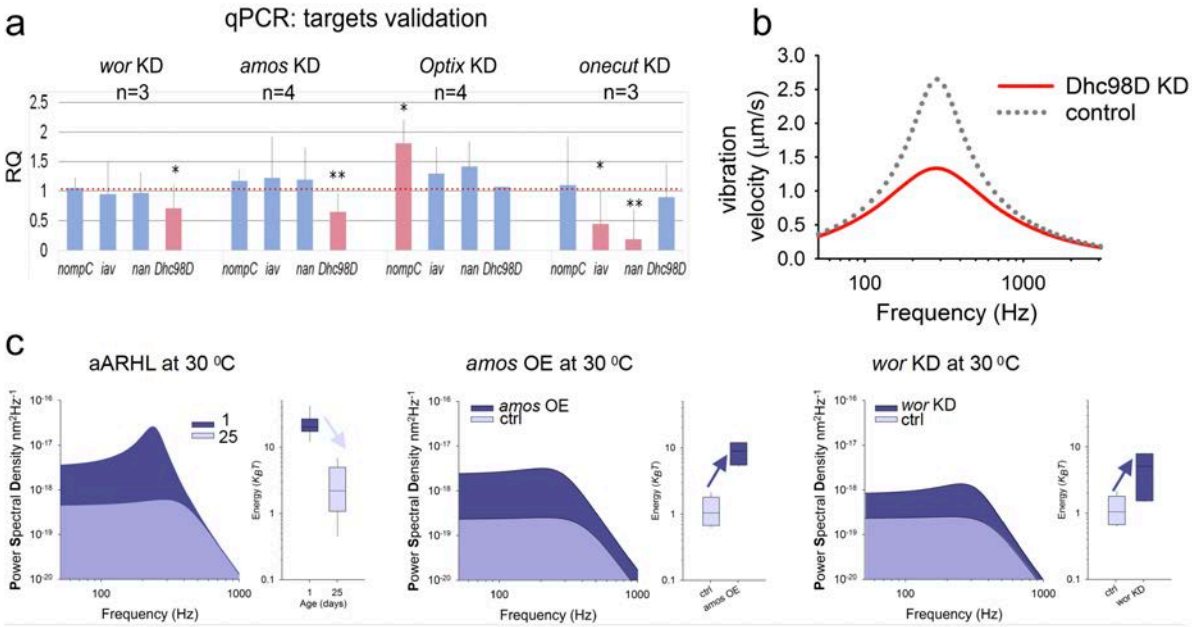
a
qPCR: targets validation
wor KD
n=3
amos KD
n=4
Optix KD
n=4
onecut KD
n=3
RQ
nompC iav nan Dhc98D
b
Dhc98D KD
control
vibration velocity (µm/s)
Frequency (Hz)
c
aARHL at 30 °C
amos OE at 30 °C
wor KD at 30 °C
Power Spectral Density nm²Hz⁻¹
Frequency (Hz)
Age (days)
amos OE
ctrl
wor KD

1182

1183

Figure 6.

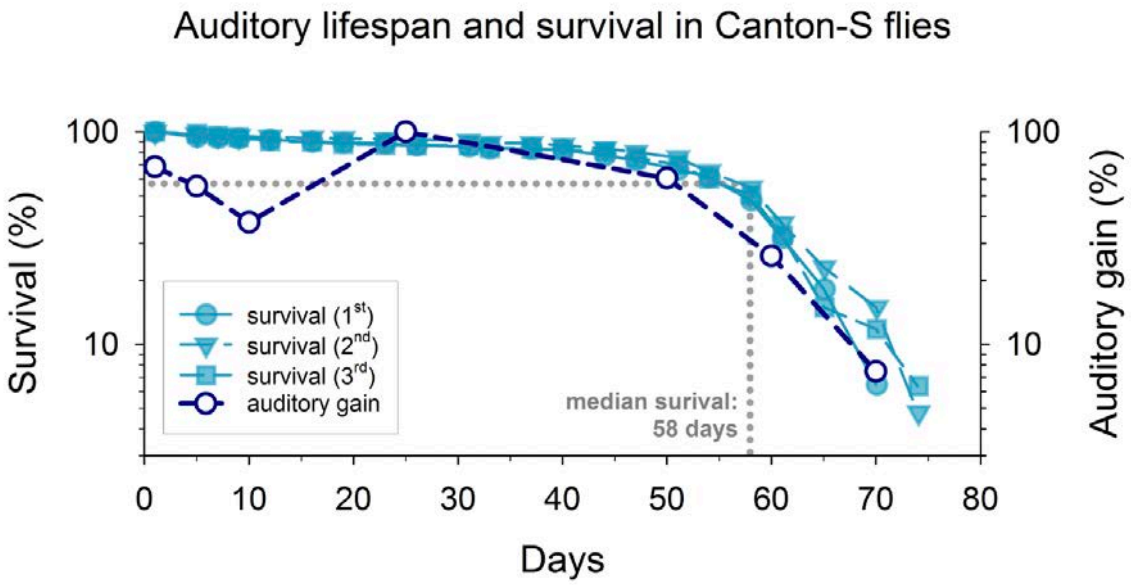

1184